Miocene to Holocene exhumation of metamorphic crustal wedges in the NW Himalaya: Evidence for tectonic extrusion coupled to fluvial erosion

Jean-Claude Vannay,[1] Bernhard Grasemann,[2] Meinert Rahn,[3,4] Wolfgang Frank,[2]
Andrew Carter,[5] Vincent Baudraz,[1] and Mike Cosca[1]

Received 24 June 2002; revised 17 August 2003; accepted 24 October 2003; published 6 February 2004.

[1] The Himalayan crystalline core zone exposed along the Sutlej Valley (India) is composed of two high-grade metamorphic gneiss sheets that were successively underthrusted and tectonically extruded, as a consequence of the foreland-directed propagation of crustal deformation in the Indian plate margin. The High Himalayan Crystalline Sequence (HHCS) is composed of amphibolite facies to migmatitic paragneisses, metamorphosed at temperatures up to 750°C at 30 km depth between Eocene and early Miocene. During early Miocene, combined thrusting along the Main Central Thrust (MCT) and extension along the Sangla Detachment induced the rapid exhumation and cooling of the HHCS, whereas exhumation was mainly controlled by erosion since middle Miocene. The Lesser Himalayan Crystalline Sequence (LHCS) is composed of amphibolite facies para- and orthogneisses, metamorphosed at temperatures up to 700°C during underthrusting down to 30 km depth beneath the MCT. The LHCS cooled very rapidly since late Miocene, as a consequence of exhumation controlled by thrusting along the Munsiari Thrust and extension in the MCT hanging wall. This renewed phase of tectonic extrusion at the Himalayan front is still active, as indicated by the present-day regional seismicity, and by hydrothermal circulation linked to elevated near-surface geothermal gradients in the LHCS. As recently evidenced in the Himalayan syntaxes, active exhumation of deep crustal rocks along the Sutlej Valley is spatially correlated with the high erosional potential of this major trans-Himalayan river. This correlation supports the emerging view of a positive feedback during continental collision between crustal-scale tectono-thermal reworking and efficient erosion along major river systems. *INDEX TERMS:* 8102 Tectonophysics: Continental contractional orogenic belts; 8110 Tectonophysics: Continental tectonics—general (0905); 8107 Tectonophysics: Continental neotectonics; 1824 Hydrology: Geomorphology (1625); 9320 Information Related to Geographic Region: Asia; *KEYWORDS:* Himalayan orogen, tectonic extrusion, tectonic geomorphology, fluvial erosion, feedback. **Citation:** Vannay, J.-C., B. Grasemann, M. Rahn, W. Frank, A. Carter, V. Baudraz, and M. Cosca (2004), Miocene to Holocene exhumation of metamorphic crustal wedges in the NW Himalaya: Evidence for tectonic extrusion coupled to fluvial erosion, *Tectonics*, *23*, TC1014, doi:10.1029/2002TC001429.

1. Introduction

[2] The long-lasting debate on the relative control of tectonic versus erosional processes on the evolution of collisional mountain belts has been stimulated by results of numerical modeling that predict that these processes are linked by a positive feedback [e.g., *Jamieson and Beaumont*, 1989; *Beaumont et al.*, 1992; *Koons*, 1995; *Koons et al.*, 2002]. Such a coupling is supported by field-based evidence demonstrating a close spatial correlation between active continental tectonics and vigorous fluvial erosion in the syntaxial extremities of the Himalayan range.

[3] At the NW extremity of the Himalaya (Figure 1), the crystalline rocks exposed in the antiformal half-window formed by the Nanga Parbat syntaxis are characterized by a very young, Pliocene to Pleistocene high-temperature/low-pressure metamorphic and anatectic activity. Geochronological and pressure-temperature (P-T) results indicate cooling rates in excess of 200°C/Myr, as well as ~15–20 km of unroofing at rates ~5 mm/yr during the past 3 Myr [*Zeitler et al.*, 2001, and references therein]. Exhumation of the Nanga Parbat massif is still active, as indicated by an intense micro-seismic activity, as well as by the shallow brittle-ductile transition beneath the massif (~2 to 5 km below sea level), and by active hydrothermal circulation, testifying to a very steep near-

[1]Institut de Minéralogie et Géochimie, Université de Lausanne, Lausanne, Switzerland.
[2]Institut für Geologie, Universität Wien, Vienna, Austria.
[3]Institut für Mineralogie, Petrologie und Geochemie, Albert-Ludwigs Universität Freiburg, Freiburg, Germany.
[4]Now at Swiss Federal Nuclear Safety Inspectorate, Villigen-HSK, Switzerland.
[5]Research School of Geological and Geophysical Sciences, Birbeck and University Colleges, London, UK.

0278-7407/04/2002TC001429

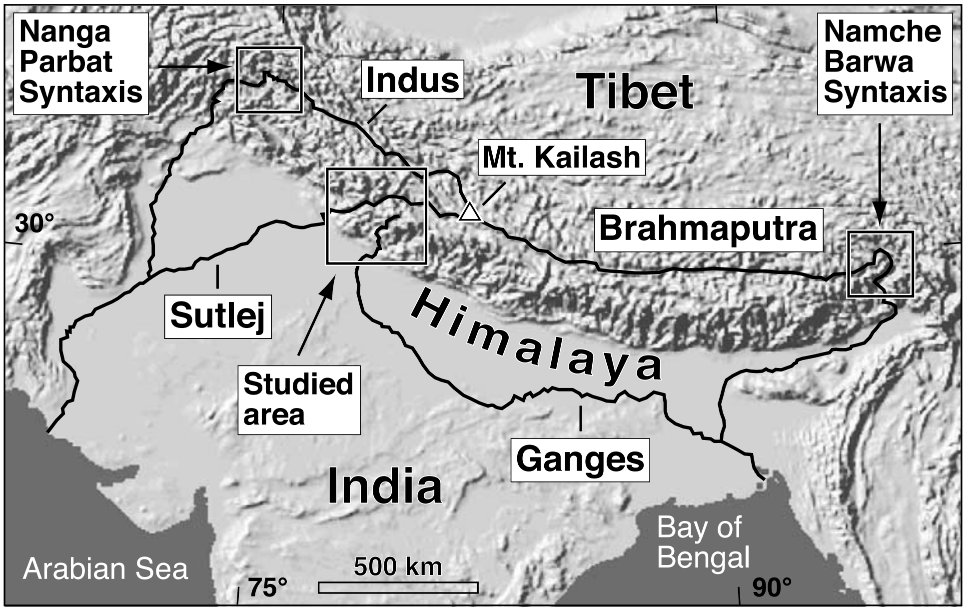

Figure 1. Geographical setting of the studied area in the Himalaya (topography based on the GTOPO30 digital elevation model, U.S. Geological Survey).

surface geothermal gradient due to heat advection [*Zeitler et al.*, 2001]. Although less studied, the Namche Barwa syntaxis (Figure 1), at the SE extremity of the range, also appears to be characterized by a comparably rapid exhumation of an antiformal high-grade metamorphic massif since Pliocene [*Burg et al.*, 1997].

[4] Both the Nanga Parbat and Namche Barwa massifs are deeply transected by the two main trans-Himalayan rivers, the Indus and the Tsangpo-Brahmaputra, respectively, that cut two of the deepest gorges on the Earth (Figure 1). Fluvial incision rates in excess of 1 cm/yr, and locally reaching $\sim$2 cm/yr, have been measured in the Nanga Parbat massif [e.g., *Burbank et al.*, 1996; *Shroder and Bishop*, 2000]. The close spatial correlation between enhanced exhumation of deep crustal rocks and intense fluvial erosion in the Himalayan syntaxes strongly suggests a positive feedback relationship between tectonic and surficial processes [*Zeitler et al.*, 2001; *Koons et al.*, 2002]. This interpretation implies that focused erosion, through rapid fluvial incision and efficient removal of eroded rocks, locally enhances isostatic and tectonic uplift, which in turn contributes to heat advection and further weakening of the crust, as well as to maintaining steep topographic gradients in the face of rapid erosion. For *Zeitler et al.* [2001], the Pliocene to present-day tectonothermal activity coupled to vigorous erosion in the Nanga Parbat syntaxis, and probably the Namche Barwa syntaxis as well, are anomalous features that stand out from the general pattern of the tectono-metamorphic evolution observed along the $\sim$2500 km belt. Thermo-mechanical modeling indicates, however, that focused erosion was most likely a key factor controlling exhumation of high-grade metamorphic thrust sheets that occur along the entire orogen between the syntaxes [*Beaumont et al.*, 2001]. Moreover, modeling of present-day rate-of-erosion indexes over the entire Himalaya [*Finlayson et al.*, 2002] indicates that, in addition to the syntaxes, discrete centers of very high fluvial erosion occur along some major watersheds of the central part of the Himalaya, notably along the Sutlej River (Figure 1).

[5] These considerations raise two interesting questions: (1) is active exhumation of metamorphic rocks coupled to efficient fluvial erosion an anomalous feature restricted to the syntaxes of the Himalayan belt, possibly as a consequence of tectonic and/or geomorphic edge effects at the corners of the Indian plate indenter [*Zeitler et al.*, 2001]? Or (2) is there evidence for comparable correlations between active tectonics and fluvial erosion along the Himalayan belt between the syntaxes?

[6] In order to address these questions, we used $^{40}Ar/^{39}Ar$ and fission tracks geochronology methods, in combination with detailed structural analyses, to constrain the exhumation history of two high-grade metamorphic thrust sheets exposed along the Sutlej, the main trans-Himalayan river between the syntaxes.

2. Geological Setting

[7] The Himalaya represents the southern border of the largest zone of active crustal deformation on the Earth, resulting from the continental collision between India and Asia since the Eocene, about 55 Myr ago [e.g., *Hodges*, 2000]. The Himalayan kinematic evolution is largely controlled by major faults, bounding the various terranes that have been gradually scraped off the underthrusting Indian plate and accreted to the orogen. The Himalaya is

thus being subdivided into several contrasting units separated by major tectonic contacts (Figure 2). From north to south, that is, from the internal to the external parts of the orogen, these units are (1) the Indus suture zone, containing the ophiolites of the Neo-Tethys ocean; (2) the Tethyan Himalaya, containing the Upper Proterozoic to Eocene sedimentary cover of the north Indian margin; (3) the Himalayan crystalline core zone, composed of high-grade metamorphic gneisses and migmatites; (4) the Lesser Himalaya, mainly composed of low-grade Proterozoic sediments of the Indian plate; and (5) the Sub-Himalaya foreland basin, containing the Oligocene to Neogene detrital sediments derived from erosion of the orogen.

[8] An increasing amount of evidence indicates that the Himalayan crystalline core zone is composed of two distinct lithotectonic units [e.g., *Valdiya*, 1980; *Srivastava and Mitra*, 1994; *Ahmad et al.*, 2000]. The upper unit is the High Himalaya Crystalline Sequence (HHCS), a thick sequence of amphibolite facies to migmatitic gneisses, bounded at its base by the Main Central Thrust (MCT; Figure 2). Beneath the MCT, the lower unit is the Lesser Himalayan Crystalline Sequence (LHCS), predominantly composed of amphibolite facies augengneisses, and bounded at its base by the Munsiari Thrust. In the NW Himalaya, these thrust sheets are exposed for a structural thickness up to 25 km along the deep cross-section cut by the Sutlej river across the High Himalayan range (Figures 2 and 3). The main features of the lithotectonic units cropping out in the Sutlej Valley are summarized in the following sections.

2.1. Lesser Himalaya

[9] The Lesser Himalaya is mainly composed of Early Proterozoic detrital sediments deposited between approximately 1900 and 1800 Ma [*Parrish and Hodges*, 1996; *Ahmad et al.*, 2000; *DeCelles et al.*, 2000], and subsequently overthrusted during the Himalayan orogenesis onto Sub-Himalaya units along the Main Boundary Thrust (MBT; Figure 2). Along the studied transect, the Lesser Himalaya sequence mainly consists of massive quartz-arenites intruded by basalts dated at 1800 ± 13 Ma [*Miller et al.*, 2000].

2.2. Lesser Himalayan Crystalline Sequence (LHCS)

[10] Overthrusting the Lesser Himalaya along the Munsiari Thrust, the LHCS unit is a medium- to high-grade metamorphic sequence derived from Lesser Himalayan lithologies. Along the Sutlej section, the LHCS crops out within a tectonic window called the Larji-Kulu-Rampur Window (LKR Window). The lower part of this unit is composed of an up to 9 km thick sequence of mylonitic micaschist and granitic gneiss, with minor metabasite and quartzite [*Vannay and Grasemann*, 1998]. The upper part of the LHCS is an up to 7 km thick sheet of penetratively deformed orthogneiss (Wangtu-Bandal granitic gneiss), derived from a Lower Proterozoic granitic protolith (zircon U-Pb age = 1840 ± 16 Ma) [*Miller et al.*, 2000]. These rocks probably represent part of the basement onto which the Lesser Himalayan sediments were deposited.

[11] To the SE of the studied area, from Garhwal to Nepal, the LHCS unit (locally known as the Munsiari Group or MCT zone) is characterized by widespread Lower Proterozoic granitic gneisses, such as the Munsiari granite dated at 1865 ± 60 Ma [e.g., *Valdiya*, 1980; *Srivastava and Mitra*, 1994; *Upreti and Le Fort*, 1999; *Catlos et al.*, 2001]. In Garhwal, the LHCS and the Lesser Himalayan sediments are characterized by a comparable Sr and Nd isotopic signature indicative of an Early Proterozoic deposition age [*Ahmad et al.*, 2000]. To the NW of the Sutlej Valley, the LHCS crops out discontinuously beneath the MCT [*Frank et al.*, 1995], and it possibly extends as far as NW Pakistan, as indicated by isotopic results demonstrating that the high-grade gneisses of the Nanga Parbat massif also originated from Lesser Himalayan lithologies [*Whittington et al.*, 2000].

2.3. High Himalayan Crystalline Sequence (HHCS)

[12] Along the entire Himalaya, the HHCS represents the main metamorphic unit forming the crystalline core zone of the orogen. The HHCS is bounded at its base by the Main Central Thrust (MCT), a major fault that accommodated up to 250 km of shortening during collision [e.g., *Hodges*, 2000]. In numerous sections across the belt, the HHCS is separated from the overlying, weakly metamorphosed sediments of the Tethyan Himalaya by extensional faults collectively referred to as the South Tibetan Detachment System (STDS) [*Burchfiel et al.*, 1992]. The main phase of tectonic exhumation of the HHCS was associated with coeval thrusting along the MCT and extension along the STDS during early Miocene [*Hodges et al.*, 1992].

[13] In some Himalayan sections, a gradual metamorphic transition is observed between the HHCS and the base of the Tethyan Himalaya [e.g., *Vannay and Steck*, 1995], and these units are characterized by comparable Sr, Nd and O isotopic signatures [*Vannay et al.*, 1999; *Ahmad et al.*, 2000; *Robinson et al.*, 2001]. The age distribution of detrital zircons indicates that the HHCS paragneisses in Nepal derived from a sedimentary sequence deposited approximately between 800 and 480 Ma [*Parrish and Hodges*, 1996; *DeCelles et al.*, 2000]. It appears consequently that the HHCS para- and orthogneisses mostly represent metamorphic equivalents of the Upper Proterozoic to Cambrian sediments forming the base of the Tethyan Himalaya, and often intruded by Cambro-Ordovician granitic plutons. Along the Sutlej section, the HHCS corresponds to a 10 km thick sequence, essentially composed of amphibolite facies to migmatitic paragneisses, with minor metabasites, calc-silicate gneisses, and granitic gneisses [*Vannay and Grasemann*, 1998].

2.4. Tethyan Himalaya

[14] The Tethyan Himalaya corresponds to a nearly continuous, Upper Proterozoic to Eocene sedimentary sequence deposited on the northern Indian margin. These

sediments generally underwent only very low-grade metamorphic conditions as a consequence of thin-skinned tectonics during the Himalayan orogenesis. Along the Sutlej section, the base of the Tethyan Himalaya consists mainly of metapelite and metapsammite derived from a thick and homogeneous sequence of Upper Proterozoic to Lower Cambrian siltstone and sandstone. These sediments are intruded by the Kinnaur Kailash Granite that yielded

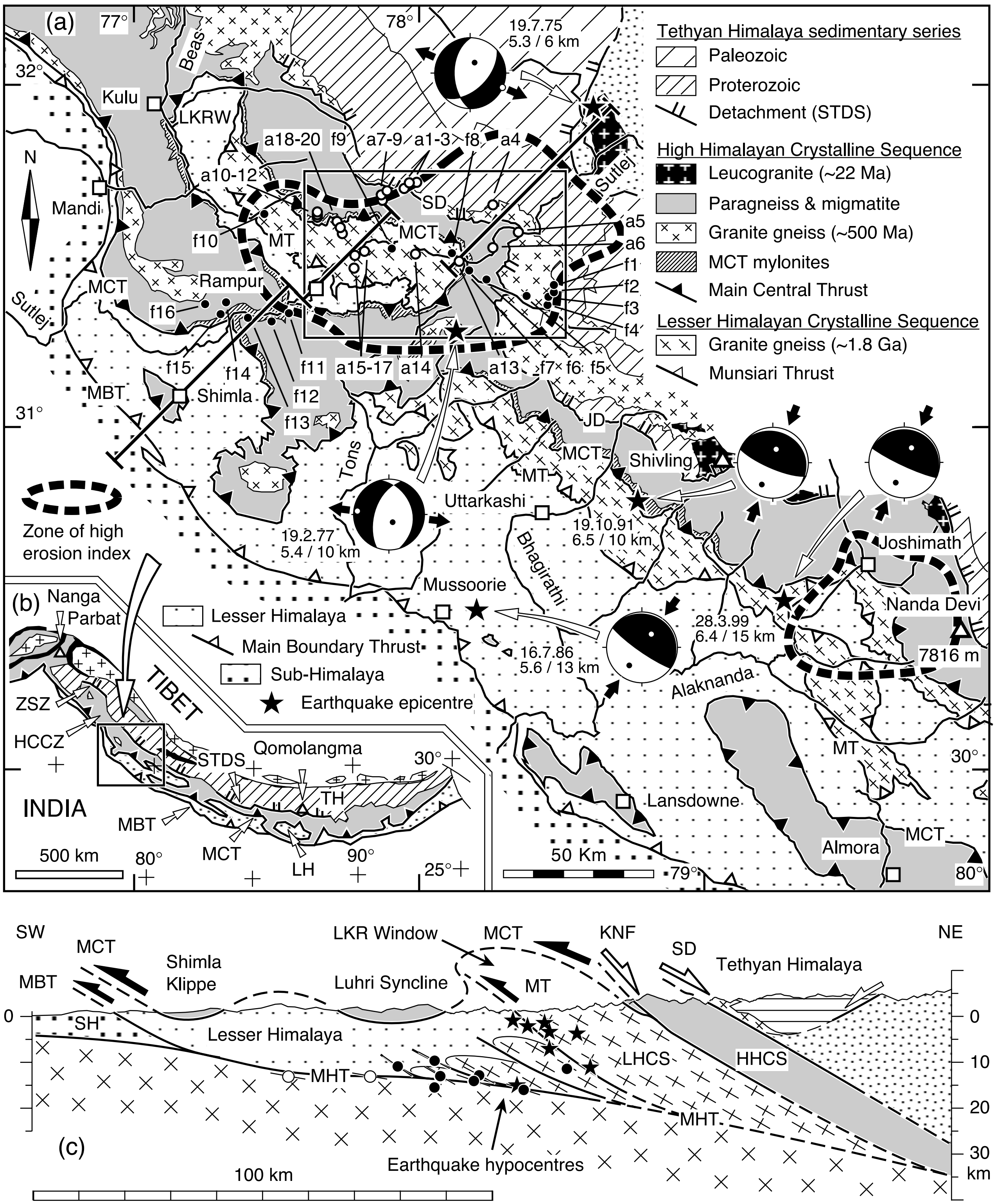

Rb-Sr ages at 453 ± 9 Ma and 477 ± 29 Ma [*Kwatra et al.*, 1999].

3. Structural Analysis

[15] The structural analysis allows constraints to be placed on the ductile to brittle kinematic evolution of the various units cropping out along the Sutlej section. The relative chronology of the polyphase structural evolution observed within each unit is well constrained by crosscutting relations, but it is more difficult to establish the temporal correlation between the deformation phases observed in the different units separated by major tectonic breaks. The progressive deformation history is consequently described and labeled separately for each unit.

3.1. Structures in the Tethyan Himalaya

[16] The base of the Tethyan Himalaya is deformed by two main phases of ductile deformation (Figure 4). The earliest deformation ($D1_T$) is responsible for a penetrative schistosity ($S1_T$), sub-parallel to the relatively well-preserved bedding (S0). The second deformation phase ($D2_T$) is responsible for the dominant penetrative schistosity ($S2_T$), generally marked by muscovite and biotite. The $D2_T$ phase is associated with a tectonic movement toward the SW, as indicated by the NE-SW oriented $L2_T$ mineral lineation, and by ubiquitous SW verging, tight to close $F2_T$ folds. The $D1_T$ deformation is interpreted to reflect an early phase of thin-skinned tectonics responsible for the low-grade metamorphism of the Tethyan sediments. The $D2_T$ deformation is associated with subsequent SW directed thrusting and folding.

[17] The brittle-ductile to brittle structures observed in the Tethyan Himalaya mainly consist of NW dipping extensional shear zones and slickensides, indicating a NW-SE oriented extension, and distributed in both the metasediments and the Kinnaur Kailash Granite (Figure 3). Some SE dipping faults are associated with fault breccia, cataclasite, and clay gouge, in which Riedel shears indicate a top-to-the-SE extension. In the granitic rocks, the cataclastic faulting commonly overprints extensional C-S fabrics, in which the dynamically recrystallized quartz preserved shape and crystallographic preferred orientations that confirm a ductile extension. These observations indicate a protracted extension, initiated in ductile to brittle-ductile conditions, and continuing during a more brittle regime.

3.2. Sangla Detachment Mylonitic Zone

[18] The Sangla Detachment separates the HHCS from the Tethyan Himalaya in the Sutlej section, and it represents thus a segment of the South Tibetan Detachment System. The Sangla Detachment corresponds to a ductile shear zone affecting the contact between the Kinnaur Kailash Granite (KKG), at the base of the Tethyan Himalaya, and the underlying migmatitic paragneiss of the HHCS (Figures 3 and 5). This shear zone is revealed by a marked strain gradient from the top to the base of the KKG. In the upper part of the KKG, the original magmatic texture is generally well preserved, and only sporadic mylonitic to phyllonitic shear zones are observed. Toward the base of the KKG, the penetrative ductile strain progressively increases. Along the lower contact of the granite, a mylonitic to ultramylonitic zone up to a few hundred meters thick is observed in places. The stretching lineation in these mylonites generally dips toward the east (Figures 3 and 5, lineation $L3_H$). Numerous shear sense criteria, such as normal drag shear bands [*Grasemann et al.*, 2003], C/S fabrics, delta-type and sigma-type K-feldspar porphyroclasts, consistently indicate a top-to-the-east extensional movement. For a few hundreds of meters just below the base of the KKG, high strain and mylonitic fabrics associated with a top-to-the-east exten-

Figure 2. Geological context of the studied area (modified after *Vannay and Grasemann* [2001], and references therein). (a) Geological map of the Himachal Pradesh-Garhwal area in the NW Himalaya of India. The location of samples analyzed for $^{40}Ar/^{39}Ar$ geochronology is given by the open circles labeled "a", whereas the solid circles labeled "f" correspond to the samples analyzed for fission track geochronology. Major earthquake epicenters in the illustrated area are indicated by stars, together with date, body wave magnitude, and approximate depth [*Molnar and Lyon-Caen*, 1989; *Kayal*, 1996; *Mahajan and Virdi*, 2001; USGS National Earthquake Information Center]. Present-day seismic activity indicates that SW directed thrusting occurs along the MBT and Munsiari Thrust, in the footwall of the inactive MCT, whereas E-W to WNW-ESE extension occurs in the MCT hanging wall, as a consequence of the east directed lateral extrusion of Tibet (fault plane solutions: solid field = contraction, solid dot = *P* axis, open dot = *T* axis). The HHCS versus LHCS origin of the crystalline thrust sheets cropping out as klippes on the Lesser Himalaya of Garhwal (e.g., Almora-Dadeldhura klippe) is constrained by isotopic results [*Ahmad et al.*, 2000; *Robinson et al.*, 2001]. The areas delimited by thick dashed lines correspond to zones of high erosion index, comparable to what is observed in the Nanga Parbat syntaxis region [*Finlayson et al.*, 2002]. (b) Generalized geological map of the Himalaya. (c) Geological cross section for the Sutlej Valley, based on the geological map, projected focal depth of earthquakes in this part of the NW Himalaya (solid circles after *Ni and Barazangi* [1984], open circles after *Molnar and Lyon-Caen* [1989], stars after *Kayal* [1996]), and seismic data for the Main Himalayan Thrust beneath the Sub-Himalaya [*Powers et al.*, 1998]. Abbreviations: HCCZ, Himalayan crystalline core zone (HHCS + LHCS); HHCS, High Himalayan Crystalline Sequence; JD, Jalha Detachment; KNF, Karcham Normal Fault; LH, Lesser Himalaya; LHCS, Lesser Himalayan Crystalline Sequence; LKRW, Larji-Kulu-Rampur Window; MBT, Main Boundary Thrust; MCT, Main Central Thrust; MHT, Main Himalayan Thrust; MT, Munsiari Thrust; NHCS, North Himalayan Crystalline Sequence; SD, Sangla Detachment; SH, Sub-Himalaya; STDS, South Tibetan Detachment System; ZSZ, Zanskar Shear Zone.

sional movement are also observed at the top of the HHCS. Sub-isoclinal to tight folds deforming the mylonitic schistosity along the HHCS-KKG contact highlight two phases of ductile deformation in the Sangla Detachment zone (Figure 5). The earlier deformation is related to a foreland-directed thrusting, as indicated by rare contractional shear sense criteria preserved in these mylonites, whereas the second deformation corresponds to the dominant extensional movement. These observations suggest that the Sangla Detachment corresponds to the reactivation of a former thrust, beneath which the HHCS was initially underthrusted and metamorphosed.

3.3. Structures in the High Himalayan Crystalline Sequence

[19] The ductile deformation in the HHCS is the consequence of two major phases, $D1_H$ and $D2_H$ (Figure 5). The relative chronology of these phases is revealed by fold interference patterns, as well as by a folded $S1_H$ schistosity

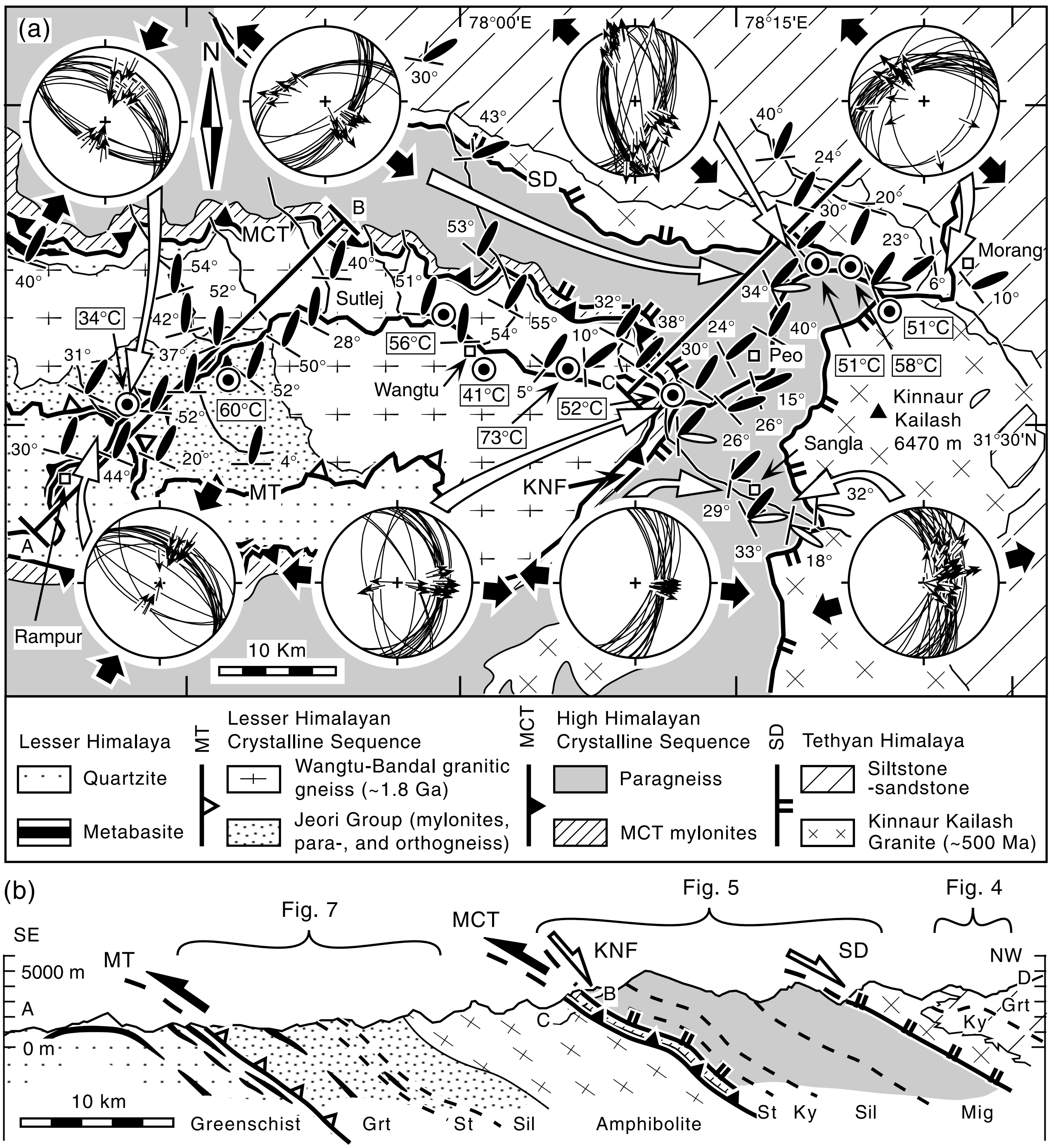

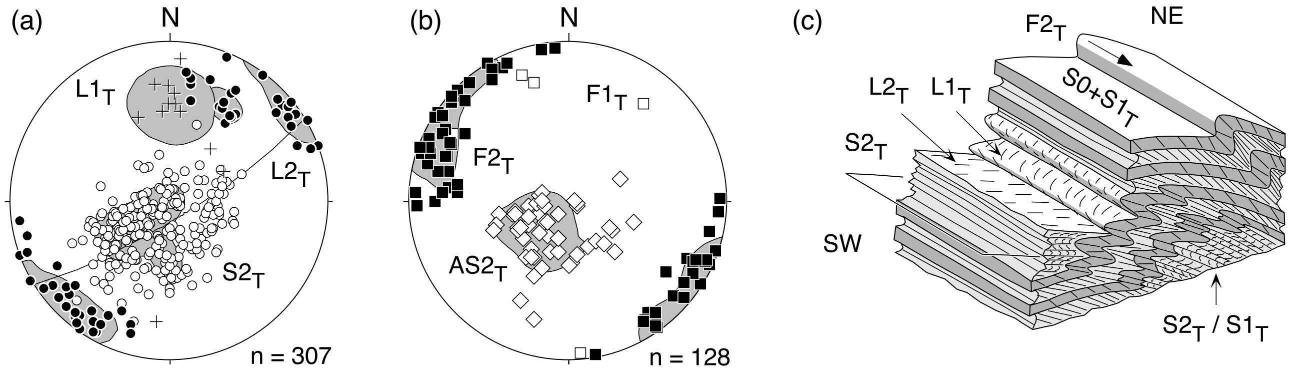

Figure 4. Ductile structures in the metasediments forming the base of the Tethyan Himalaya along the upper Sutlej Valley. (a) Orientations of the penetrative schistosity and mineral lineation, projected in equal-area stereograms (lower hemisphere, shaded areas = five times random distribution). Average orientation of the main penetrative fabrics: $S2_T$ = 027/17 and $L2_T$ = 042/03. (b) Orientations of the folds axes and axial surfaces. Abbreviations: S, schistosity; L, mineral or stretching lineation; F, fold axis; AS, fold axial surface. (c) Synoptic perspective diagram summarizing the style and relations of the various structures (variable scale).

in the hinge zone of sub-isoclinal to tight $F2_H$ folds. Larger amplitude, isoclinal $F1_H$ folds (Figure 6a) have axial orientations parallel to the $L2_H$ mineral lineation, suggesting a re-orientation of $D1_H$ structures during the dominant $D2_H$ phase. Sheath folds, probably resulting from the amplification of $F1_H$ folds during the $D2_H$ phase, illustrate the high shear strain recorded by the HHCS rocks. The penetrative schistosity $S2_H$, as well as the $L2_H$ lineation, dip about 30° toward the NE. Throughout most of the HHCS, the $D2_H$ phase is associated with a foreland-directed movement toward the SW, as constrained by various shear sense criteria (Figure 6b). In a restricted zone at the top of the HHCS, however, the deformation $D2_H$ is associated with the extensional movement in the Sangla Detachment mylonitic zone. The $D2_H$ phase is interpreted to record the ductile stage of exhumation of the HHCS, controlled by combined SW directed thrusting along the MCT and east directed extension along the Sangla Detachment [*Vannay and Grasemann*, 2001]. Although this deformation was strongly non-coaxial, conjugate sets of normal and reverse drag shear bands, as well as a-Type flanking folds, indicate a significant component of pure shear during the $D2_H$ phase [*Grasemann et al.*, 2003]. The $D1_H$ phase is most likely associated with the initial underthrusting of the HHCS beneath the Tethyan Himalaya.

[20] Throughout the HHCS, the contractional ductile fabrics are overprinted by brittle-ductile to brittle extensional structures (Figure 6c). Riedel shears and slickenfibers indicate a predominantly E-W to NW-SE oriented brittle extension, whereas a NNW-SSE oriented dextral strike slip movement occurred locally (Figure 3).

3.4. MCT Mylonitic Zone

[21] In the internal part of the orogen along the Sutlej section, the MCT is marked by a 1 to 2 km thick mylonitic zone separating the Wangtu-Bandal granitic gneiss from the overlying HHCS paragneisses (Figures 2 and 3). The SW directed thrusting movement is particularly well recorded by normal drag shear bands, C-S fabrics, and K-feldspar sigma clasts in the granitic gneisses and dark phyllonitic schists composing this mylonitic zone (Figure 5). The contractional $D2_H$ mylonitic structures of the MCT zone are superposed by extensional normal drag shear bands associated with an

Figure 3. (a) Geological map of the upper Sutlej Valley showing relevant structural orientations. The geology is modified after *Vannay and Grasemann* [1998]. The solid ellipses indicate the orientation of the penetrative mineral lineation associated with foreland-directed ductile shearing (the shape of the ellipses is fixed). Open ellipses indicate the orientation of a later mineral lineation associated with east directed ductile extension in the HHCS. The stereograms summarize the fault-slip analysis of brittle structures. The orientation of brittle faults is represented by the great circles, whereas the small arrows indicate the direction of slip, as recorded by slickensides. The large solid arrows indicate the average orientation of the horizontal component of tectonic movement, as deduced from the fault-slip analysis. Brittle deformation is characterized by a protracted NNE-SSW contraction at the level of the Munsiari Thrust, and by an E-W to NW-SE extension distributed in the hanging wall of the MCT. The circled solid dots indicate the location of hydrothermal springs [*Srikantia and Bhargava*, 1998]. (b) Geological section showing the metamorphic zonation. Barrovian metamorphic mineral zones in metapelites: Grt, garnet; St, staurolite; Ky, kyanite; Sil, sillimanite+kyanite; Mig, kyanite + sillimanite bearing migmatite. Metamorphic assemblages in the metabasites of the Lesser Himalaya and Wangtu granitic gneiss indicate greenschist and amphibolite facies conditions, respectively. Other abbreviations are as in Figure 2.

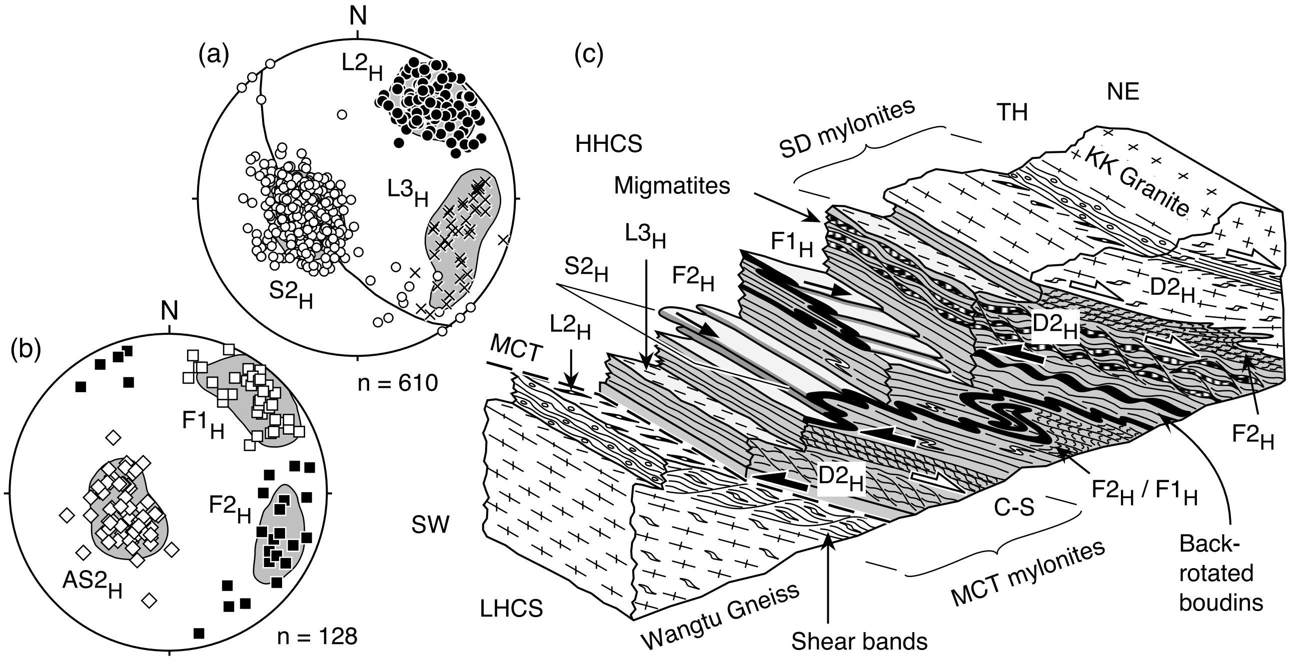

Figure 5. Ductile structures in the HHCS along the upper Sutlej Valley [after *Vannay and Grasemann*, 2001]. (a) Orientations of the penetrative schistosity and mineral lineation, projected in equal-area stereograms (lower hemisphere, shaded areas = five times random distribution). Average orientation of the main penetrative fabrics: $S2_H$ = 055/28 and $L2_H$ = 038/24. (b) Orientations of the folds axes and axial surfaces. Abbreviations are as in Figure 4. (c) Synoptic perspective diagram summarizing the style and relations of the various structures (variable scale). (Reproduced with permission from Cambridge University Press.)

east dipping mineral lineation ($L3_H$). These structures mark the onset of a late phase of east directed extension, subsequently evolving to a more brittle extension. It is worth emphasizing that no significant contractional brittle overprint is observed in the MCT zone of the Sutlej valley. In the more frontal part of the orogen, the MCT zone is composed of an up to 1.5 km thick mylonitic orthogneiss, folded around the Larji-Kulu-Rampur Window [*Frank et al.*, 1995]. These rocks yielded a Rb-Sr whole rock age at 1840 ± 70 Ma, indicating that they were derived from the same Lower Proterozoic granitic protolith as the Wangtu-Bandal orthogneiss [*Miller et al.*, 2000]. This result suggests that thrusting of the HHCS paragneisses along the MCT also involved slices of the granitic basement of the Indian plate. A quantitative kinematic analysis of quartz microfabric and flanking structures in these mylonites at the base of the Luhri syncline (Figure 2) indicates that ductile deformation during SW directed thrusting involved a combination of both simple and pure shear [*Grasemann et al.*, 1999].

3.5. Karcham Normal Fault

[22] The Karcham Normal Fault (KNF) corresponds to a cataclastic extensional fault crosscutting the MCT mylonites a few hundred of meters above the base of the HHCS in the Sutlej Valley (Figure 3) [*Janda et al.*, 2002]. This fault is marked by a 100 m thick zone of cataclasites to ultracataclasites containing slickenfibers, Riedel shears, and en echelon tension gashes indicating a top-to-the-east extension (Figure 2). The KNF is clearly kinematically related to the brittle extensional structures distributed throughout the HHCS. We interpret the KNF as an extensional fault cutting at the level of the MCT zone during the tectonic exhumation of the underlying LHCS.

3.6. Structures in the Lesser Himalayan Crystalline Sequence

[23] Two phases of ductile deformation affected the LHCS gneisses. The dominant ductile deformation corresponds to a $D2_L$ phase, responsible for a penetrative schistosity $S2_L$ and mineral lineation $L2_L$, both generally dipping toward the NNE to NE (Figures 3 and 7). Numerous shear sense criteria indicate that the $D2_L$ deformation is associated with a foreland-directed, top-to-the SW thrusting. Sub-isoclinal to tight $F2_L$ folds deform an older $S1_L$ penetrative schistosity, probably related to the initial underthrusting of the LHCS beneath the MCT. The $D2_L$ phase is interpreted to record the exhumation of the LHCS, induced by SW directed thrusting along the Munsiari Thrust. A late phase of ductile deformation $D3_L$ is responsible for chevron-type folds ($F3_L$) deforming the main penetrative schistosity ($S2_L$; Figure 7). In contrast to the MCT hanging wall,

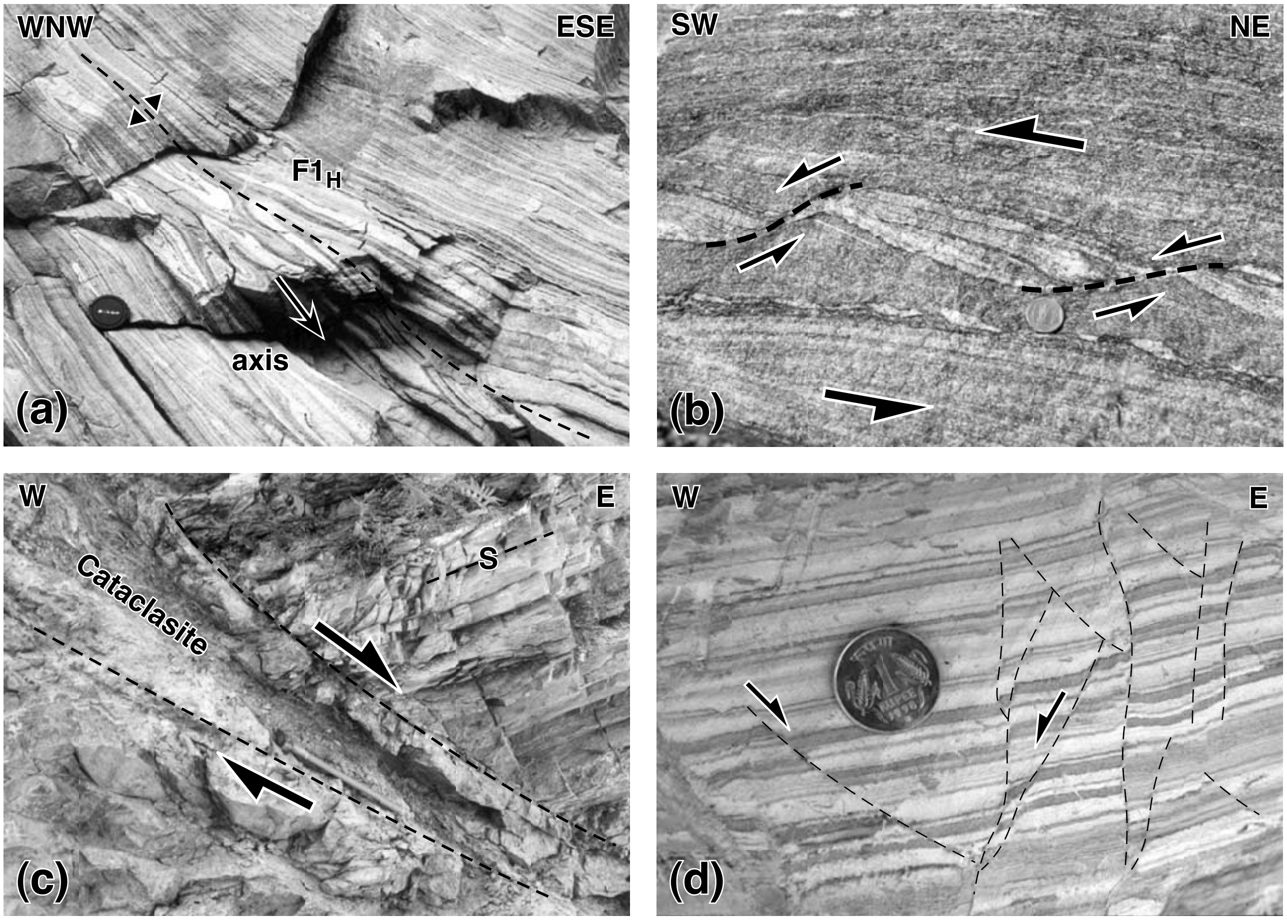

Figure 6. Representative structures from the Sutlej section. (a) Large-amplitude, sub-isoclinal $F1_H$ folds in the HHCS paragneiss of the Baspa Valley west of Sangla (arrow = axial orientation; dashed line = axial trace; lens cover = 6 cm). (b) Normal drag shear band boudinage in the HHCS paragneiss of the Sutlej Valley south of Peo. If such structures are stable during progressive deformation, they indicate a SW directed non-coaxial flow with a high pure shear component [*Grasemann et al.*, 2003] (coin = 2.8 cm). (c) Cataclastic fault accommodating east directed extension in the HHCS paragneiss of the Baspa Valley west of Sangla (S = schistosity; hammer = 50 cm). (d) Syn-sedimentary faults recording E-W extension in rockfall-dammed lake sediments in the Baspa Valley south of Sangla. ^{14}C dating indicate a Holocene age at ~5300 years before present for these sediments (unpublished data by E. Draganits).

no significant extensional brittle overprint is observed in the LHCS (Figure 3).

3.7. Munsiari Thrust Mylonitic Zone

[24] The base of the LHCS unit in the Sutlej Valley corresponds to a 1 to 2 km thick sheet of mylonitic granitic gneisses and phyllonites related to the Munsiari Thrust. Beneath this thrust, a mylonitic fabric is observed for some hundreds of meters at the top of the Lesser Himalaya unit. A penetrative NNE dipping lineation (Figure 3) and several kinematic indicators, including shape and crystallographic preferred orientations in quartzitic levels, consistently indicate a top-to-the-SSW sense of shear (Figure 7).

[25] A strong brittle-ductile to brittle overprint on the Munsiari Thrust mylonites is recorded by conjugate NNE and SSW dipping reverse faults containing fault breccia, cataclasite, and fault gouge. Riedel shears, slickensides, conjugate kink bands, fault-related folds leading to duplex structures and antiformal stacks, all indicate a SSW directed contraction (Figure 3). This phase of brittle deformation records protracted thrusting along the Munsiari Thrust in shallow structural levels, during exhumation of the LHCS. The ductile to brittle tectonic evolution in the Lesser Himalayan units remained contractional, in contrast to what is observed in the MCT hanging wall.

3.8. Structures in the Lesser Himalaya

[26] The main ductile deformation in the Lesser Himalaya is marked by a penetrative, NE dipping schistosity $S1_R$, parallel to the bedding (S0), as well as by a mineral lineation $L1_R$, developed during greenschist facies conditions (Figure 7). This deformation most likely reflects the

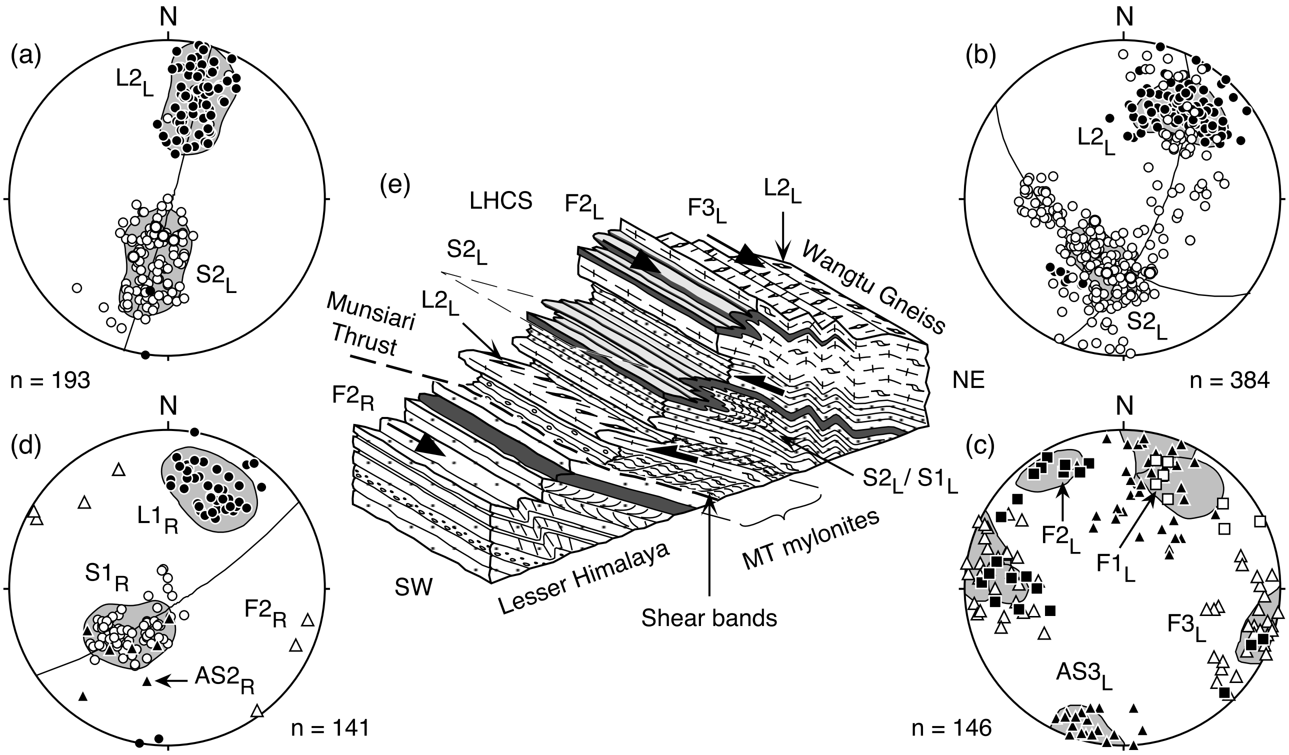

Figure 7. Ductile structures in the Lesser Himalayan units along the upper Sutlej Valley. (a) Orientations of the penetrative schistosity and mineral lineation in the paragneiss of the lower LHCS, projected in equal-area stereograms (lower hemisphere, shaded areas = five times random distribution). Average orientation of the main penetrative fabrics: $S2_L$ = 012/35 and $L2_L$ = 016/33. (b) Orientations of the penetrative schistosity and mineral lineation in the orthogneiss of the upper LHCS (Wangtu orthogneiss). Average orientation of the main penetrative fabrics: $S2_L$ = 020/33 and $L2_L$ = 035/30. (c) Orientations of the folds axes and axial surfaces in the LHCS. (d) Structural orientations in the upper part of the Lesser Himalaya (Rampur Quartzite). Average orientation of the main penetrative fabrics: $S2_R$ = 041/30 and $L2_R$ = 023/30. Abbreviations are as in Figure 4. (e) Synoptic perspective diagram summarizing the style and relations of the various structures (variable scale).

underthrusting of this unit beneath the Munsiari Thrust, as indicated by C-S fabrics and normal drag shear bands preserved in micaceous levels and indicating a top-to-the-SW sense of shear. The main penetrative foliation is deformed by late SW verging folds ($F2_R$), associated with a weak crenulation cleavage, and indicating protracted SW directed shortening during cooling (Figure 7).

4. Metamorphic Evolution

[27] The metamorphic evolution of the various units cropping out along the Sutlej section is constrained by petrographic, thermobarometry, oxygen isotope thermometry, and P-T path results. A detailed account of this metamorphic evolution is given by *Vannay and Grasemann* [1998, 2001] and *Vannay et al.* [1999], and only a summary of the relevant results is presented here. The crystalline units of the Sutlej section are characterized by typical inverted metamorphic field gradients. In the HHCS, this inverted metamorphism is revealed by a gradual superposition of staurolite, kyanite, sillimanite, and migmatite mineral zones, from the base to the top of the unit (Figure 3b). In the lower part of the LHCS, a gradual superposition of garnet, staurolite, and sillimanite mineral zones is observed, whereas mafic dykes in the overlying Wangtu granitic gneiss contain amphibolite facies assemblages. In the footwall of the Munsiari Thrust, the intrusive metabasites in the Lesser Himalaya contain greenschist facies assemblages. In the hanging wall of the Sangla Detachment, the metasediments in the lowermost part of the Tethyan Himalaya contain assemblages of the kyanite and garnet zones, and the metamorphic conditions rapidly decrease toward the north. Multiple equilibria thermobarometry and oxygen isotope thermometry indicate peak temperatures increasing from $\sim$600 to 750°C from the base to the top of the HHCS, and that these peak conditions were reached at an almost constant pressure around 8 kbar. For a lithostatic gradient of 0.27 kbar/km, this pressure translates to a burial depth around 30 km. Peak conditions in the underlying LHCS were also reached at about 30 km depth ($\sim$8 kbar) and the peak temperatures increase up-section from $\sim$600 to 700°C in the lower LHCS unit.

[28] Thermobarometry and P-T path results suggest that the tectono-thermal evolution of the HHCS can be subdivided into three main stages [*Vannay and Grasemann*, 2001]. During the initial stage, the HHCS rocks were underthrusted down to ~30 km depth (8 kbar), where the top of the unit reached temperatures up to about 600°C. The subsequent stage corresponded to a tectonically inactive period, allowing the isotherms initially perturbed by the underthrusting movement to relax toward a stable, subhorizontal thermal structure. This relaxation induced the isobaric heating of the HHCS rocks remaining at the same depth, and the peak conditions were reached as the temperature increased up to about 600°C at the base of the unit, whereas temperatures up to about 750°C triggered partial melting at the top of the unit. During the third stage, combined thrusting along the MCT and extension along the Sangla Detachment induced the rapid exhumation of the HHCS. The metamorphic peak was directly followed by cooling during decompression, implying a lack of significant thermal relaxation during exhumation. This retrograde P-T evolution reflects thus a rapid cooling of the HHCS gneiss sheet, as a consequence of underthrusting beneath the MCT of colder rocks from shallower structural levels [*Vannay and Grasemann*, 2001]. This rapid cooling did not allow the HHCS rocks to record high T/low P conditions, such as observed at the top of thicker sections across the HHCS (e.g., cordierite or andalusite-bearing assemblages) [*Dèzes et al.*, 1999]. No P-T path results are available for the LHCS, but the comparable peak P-T conditions and the lack of retrograde high T/low P overprint suggest a tectono-thermal evolution comparable to the one determined for the HHCS.

5. Geochronology

5.1. Age of Metamorphic Peak

[29] Preliminary Th-Pb dating of monazites from the HHCS of the Sutlej section yielded ages ranging from 39.6 ± 2.8 to 22.8 ± 0.4 Ma (E. Carlos, personal communication). These ages indicate that the timing of prograde metamorphism and peak conditions in the HHCS of the Sutlej is comparable to what is observed in adjacent regions to the NW and to the east. In the HHCS of Zanskar and Garhwal, the prograde evolution took place between ~33 and 28 Ma [*Vance and Harris*, 1999], and between ~44 and 25 Ma [*Foster et al.*, 2000], respectively. Numerous geochronological results all along the range show that the metamorphic peak in the HHCS was reached during early Miocene at around 23 Ma [e.g., *Dèzes et al.*, 1999; *Searle et al.*, 1999].

[30] For the LHCS of the Sutlej section, preliminary Th-Pb ages of monazites included in garnet and staurolite range from 9.9 ± 0.2 to 6.4 ± 0.5 Ma (E. Carlos, personal communication). These results are consistent with an increasing number of monazite Th-Pb crystallization ages ranging from ~10 to 6 Ma in the lower LHCS from Garhwal to Nepal [*Catlos et al.*, 2001, and references therein]. One sample from the LHCS of the Sutlej section yielded two garnet Sm-Nd ages at 11.0 ± 1.1 and 6.8 ± 1.1 Ma (C. Hager and C. Janda, personal communication). These results consistently indicate that metamorphic peak conditions in the LHCS were reached during late Miocene, between circa 11 and 6 Ma.

5.2. $^{40}Ar/^{39}Ar$ Geochronology

5.2.1. Analytical Procedure

[31] Muscovite concentrates from 20 samples (Figure 2a) were obtained by standard separation techniques. The mineral concentrates, together with standards, were analyzed by step heating at the laboratories for geochronology at the University of Vienna (9 samples) and at the University of Lausanne (11 samples), after irradiation in the Astra reactor (Seibersdorf) and Triga reactor (Denver), respectively. All data were corrected for blank, mass discrimination, post-irradiation decay, and interfering reactions before calculation of ages according to *Dalrymple et al.* [1981]. The irradiation J-values were determined with international standards including muscovite Bern 4M [*Burghele*, 1987] and Fish Canyon sanidine [*Renne et al.*, 1994]. More detailed descriptions of the $^{40}Ar/^{39}Ar$ analytical techniques followed in Vienna and Lausanne are presented by *Frimmel and Frank* [1998] and *Cosca et al.* [1998], respectively.

5.2.2. $^{40}Ar/^{39}Ar$ Results

[32] The muscovite $^{40}Ar/^{39}Ar$ release spectra diagrams are presented in Figure 8, and the detailed step heating results are given in the auxiliary material[1]. Out of 20 samples, 15 yielded well-constrained plateau ages constrained by ~60 to 85% of the released ^{39}Ar, and providing robust estimates of the muscovite cooling ages. Inverse isochron diagrams indicate that the initial $^{36}Ar/^{40}Ar$ ratios of these samples are, within uncertainties, similar or close to the present-day atmospheric value (295.5). Although they did not yield true plateau ages, two samples (a5 and a17) show homogeneous release spectra, characterized by incremental ages remaining within less than 7% of the integrated ages. Three samples (a10 to a12) yielded slightly more complex release spectra, possibly affected by impurities and/or excess ^{40}Ar in the low temperatures steps. The integrated ages for these samples are nevertheless considered as geologically meaningful, as they are consistent with the regional cooling pattern revealed by the better constrained plateau ages.

[33] The $^{40}Ar/^{39}Ar$ cooling ages are reported in Figure 9 as a function of the projected structural position of the samples along the studied section. These results reveal a striking contrast in cooling ages across the MCT. In the MCT hanging wall, cooling below the closure temperature for Ar diffusion in muscovite took place between 19.23 ± 0.14 and 17.2 ± 0.08 Ma in the lowermost Tethyan Himalaya, and between 17.65 ± 0.07 and 15.4 ± 0.07 Ma in the HHCS (Figures 8 and 9). In good agreement with comparable results from adjacent areas [e.g., *Metcalfe*, 1993], such a Miocene cooling is consistent with the exhumation of the HHCS and Tethyan Himalaya controlled by thrusting along the MCT since ~23 Ma [e.g., *Hubbard and Harrison*, 1989; *Coleman*, 1998]. In the MCT footwall, in contrast, the $^{40}Ar/^{39}Ar$ ages from the LHCS indicate cooling between 6.59 ± 0.05 and 4.29 ± 0.04 Ma (Figures 8 and 9). This late Miocene to early

[1]Supporting materials are available at ftp://ftp.agu.org/apend/tc/2002TC001429.

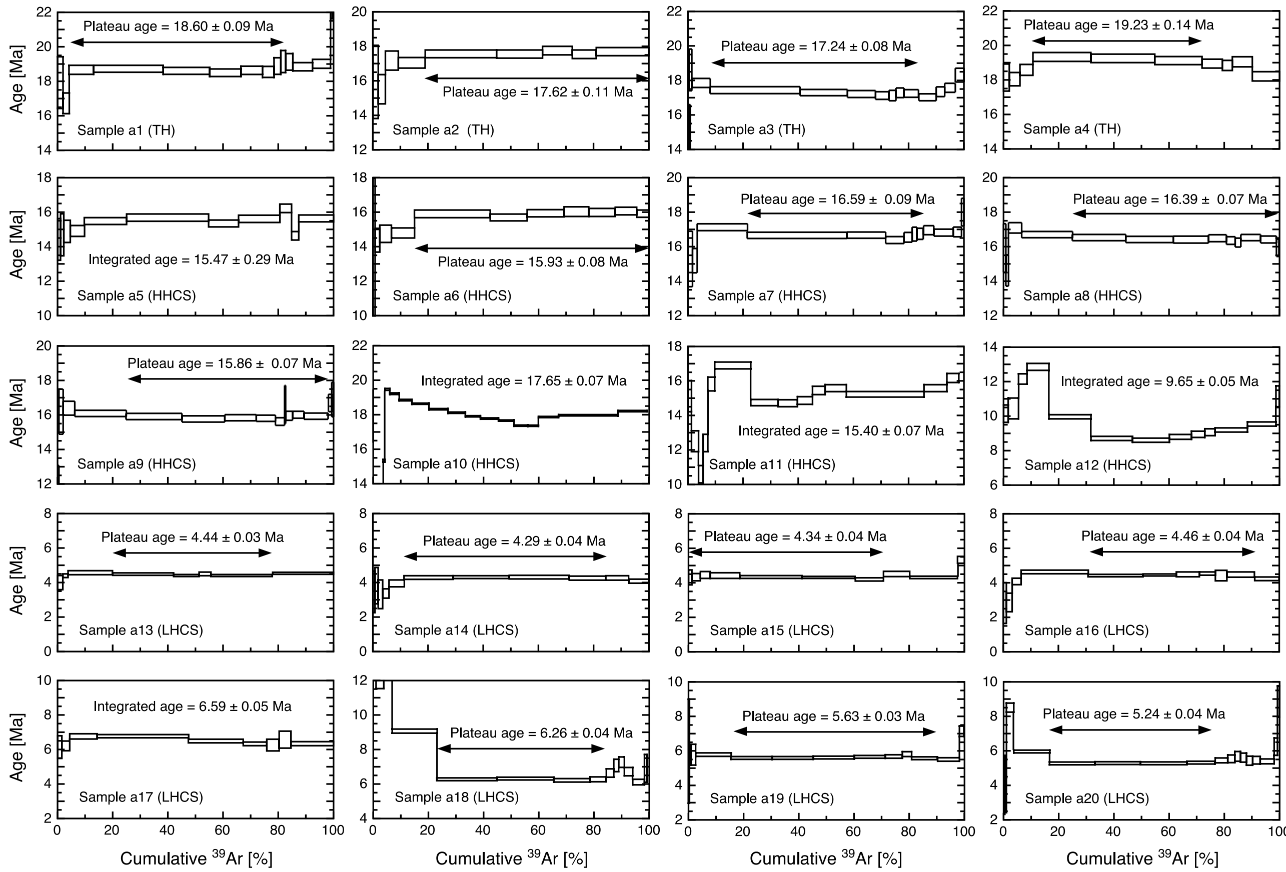

Figure 8. $^{40}Ar/^{39}Ar$ age spectra for the Sutlej section. All uncertainties are at the 2 sigmas level (95% confidence). Plateau ages correspond to the weighted mean age of at least three consecutive steps characterized by similar ages within 2 sigmas errors and representing at least 50% of the released ^{39}Ar. Sampling localities are given in Figure 2a.

Pliocene cooling indicate that the exhumation of the LHCS, controlled by thrusting along the Munsiari Thrust, is a significantly younger tectono-thermal event compared to the syn-MCT event.

5.3. Fission Track Geochronology

5.3.1. Analytical Procedure

[34] Apatite and zircon concentrates from 16 samples (Figure 2a) were obtained by standard grinding, heavy liquid, and magnetic separation procedures. Apatites were mounted within epoxy, polished, and etched with 5N HNO_3 at 20°C for 20 s. Zircons were mounted in FEP teflon, polished, and etched within a eutectic NaOH-KOH melt. Samples were irradiated at the RISØ reactor (Denmark) together with low-U muscovite as external detectors and CN5/CN2 dosimeter glasses. In muscovite, tracks were etched with concentrated HF for 35 minutes at 20°C. Central ages and their relative errors were calculated using the zeta approach [*Hurford and Green*, 1983]. Only crystals with prismatic sections parallel to the crystallographic *c* axis were accepted for analysis. Apatite composition was monitored using track etch pit size [*Burtner et al.*, 1994]. Because most samples have a low track density, only four apatite and one zircon samples yielded meaningful numbers of confined track length measurements.

5.3.2. Fission Track Results

[35] Out of 16 rock samples, 15 apatite and 14 zircon FT ages (including 13 age pairs) were measured (Table 1). These results are reported in Figure 9 as a function of their projected sample structural position, together with additional FT ages by *Jain et al.* [2000]. In the Kinnaur Kailash Granite, at the base of the Tethyan Himalaya, zircon FT ages range between 16.3 ± 1.6 and 13.6 ± 1.3 Ma, whereas apatite FT ages vary between 4.9 ± 0.8 and 2.6 ± 1.2 Ma (Figure 9). The track length distributions in apatites are unimodal and characterized by a mean track length around 14 μm, consistent with uninterrupted cooling (Table 1). These results are comparable to fission track ages from the Shivling and Gangotri leucogranites at the base of the Tethyan Himalaya in the Bhagirathi section, 70 km to the SE of the Sutlej (Figure 2) [*Sorkhabi et al.*, 1996; *Searle et al.*, 1999]. Zircon FT ages from the HHCS in the frontal part of the range (Luhri Syncline) vary between 12.2 ± 1.3 and 10.7 ± 1.1 Ma, whereas apatite FT ages range between 4.1 ± 1.6 and 3.0 ± 1.4 Ma (Figure 9). In the internal part of the range, the HHCS yielded two apatite FT ages at

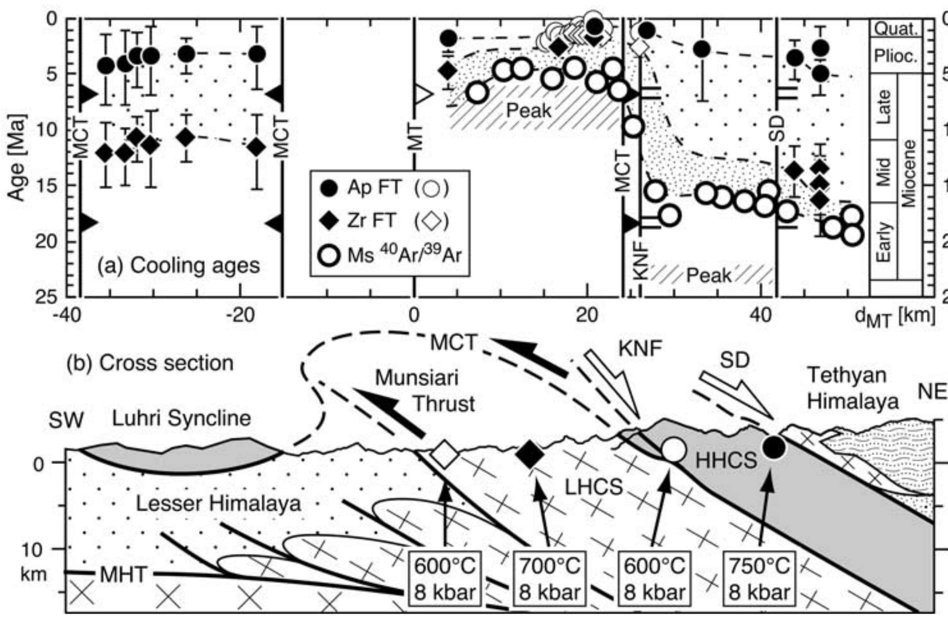

Figure 9. (a) Cooling ages profile for the Sutlej section, based on muscovite (Ms) $^{40}Ar/^{39}Ar$ ages, as well as zircon and apatite fission track results (Zr FT and Ap FT, respectively). Fission track results from the present study correspond to solid symbols, whereas open symbols represent the results by *Jain et al.* [2000]. The horizontal distance along the cross section (d_{MT}) is given relative to the Munsiari Thrust. (b) Cross section for the Sutlej traverse (no vertical exaggeration), with representative peak pressure and temperature conditions in the crystalline units after *Vannay et al.* [1999] and *Vannay and Grasemann* [2001]. Abbreviations and tectonic unit patterns are as in Figure 2.

2.7 ± 1.8 and 0.9 ± 0.4 Ma, respectively. The latter age has been obtained for a sample collected near the Karcham Normal Fault at the base of the HHCS (sample f7), in the vicinity of a hot source. This very young apatite FT age could thus reflect a late hydrothermal heating and it will not be considered in the discussion of cooling rates. Compared to the units forming the MCT hanging wall, the LHCS rocks of the LKR Window are characterized by significantly younger FT ages. Two samples from the Wangtu-Bandal granitic gneiss, and one sample from the lower part of the LHCS, yielded zircon FT ages between 4.8 ± 0.8 and 1.7 ± 0.3 Ma, and apatite FT ages between 1.7 ± 0.3 and 0.7 ± 0.6 Ma. Our FT results for the Wangtu-Bandal granitic gneiss confirm the young Pliocene to Pleistocene cooling of this unit evidenced by *Jain et al.* [2000]. For the lower part of the LHCS, however, *Jain et al.* [2000] measured apatite FT ages at ∼4.2–5.1 Ma, that is about 3 Myr older than in the Wangtu-Bandal granitic gneiss. Because these ages are similar to our $^{40}Ar/^{39}Ar$ muscovite ages, they are not considered in our cooling age profile.

5.4. Cooling and Exhumation Rates

[36] In order to estimate cooling rates, and considering the rapid cooling of the studied units, zircon and apatite fission track ages were assumed to correspond to total annealing temperatures at 290 ± 30°C and 110 ± 10°C, respectively [*Tagami et al.*, 1998; *Rahn and Grasemann*, 1999]. For the grain size range of the analyzed muscovite samples, a closure temperature for Ar diffusion at 450 ± 50°C has been calculated following *Kirschner et al.* [1996]. On the basis of weighted average ages from the Sutlej the cooling evolution of the studied units is illustrated in Figure 10.

[37] The calculation of cooling and exhumation rates from geochronological data is not straightforward, considering that the thermal structure during active orogenic processes is not steady state, and given that strong topographic gradients can significantly influence the near surface geotherm [e.g., *Mancktelow and Grasemann*, 1997]. Furthermore, numerical thermal models have shown that small changes in model input parameters (e.g., two-dimensional fault geometry, slip rate, lower boundary condition) can produce large variations in the predicted thermal history [e.g., *Ruppel and Hodges*, 1994]. Keeping these limitations in mind, cooling curves and exhumation rates were calculated using a simple analytical one-dimensional solution of the heat diffusion equation, in order to consider the influence of heat advection during exhumation [*Mancktelow and Grasemann*, 1997]. The parameters used for modeling are the surface temperature [0°C], thermal diffusivity [1×10^{-6} m^2 s^{-2}], volumetric heat production at the surface [1×10^{-6} W m^{-3}], depth at which heat production exponentially drops to 1/e [30 km], heat capacity [1100 J kg^{-1}°C^{-1}], density [2800 kg m^{-3}], and a fixed temperature lower boundary of 800°C at 40 km depth [*Harrison et al.*, 1998]. The technical details of the program code we used are given by *Mancktelow* [1998].

Table 1. Apatite and Zircon Fission Track Results for the Sutlej Section

	Sample[a]	Unit	Min[b]	Nb[c]	Spontaneous[d] ρ_s	Spontaneous[d] N_s	Induced[d] ρ_i	Induced[d] N_i	$P\chi^2$,[e] %	Dosimeter[d] ρ_d	Dosimeter[d] N_d	Age,[f] Ma	MTL,[g] µm	SD[h]	Nb.Tracks
f1	(HB25/97)	TH	Ap	20	0.119	163	4.24	5822	50	1.022	3178	4.9 ± 0.8	14.0 ± 0.26	1.33	100
			Zr	20	2.54	1445	4.89	2785	<5	0.433	2165	14.9 ± 1.4	–	–	–
f2	(HB26/97)	TH	Ap	10	0.049	23	3.36	1566	44	1.023	3180	2.6 ± 1.2	–	–	–
			Zr	20	2.64	1616	4.97	3038	<5	0.433	2165	15.3 ± 1.4	–	–	–
f3	(HB27/97)	TH	Ap	20	0.082	122	5.52	8272	11	1.025	3183	2.6 ± 0.5	14.07 ± 0.46	1.45	39
			Zr	20	3.05	1176	5.39	2077	<5	0.433	2165	16.3 ± 1.6	–	–	–
f4	(HB28/97)	TH	Ap	20	0.154	195	6.19	7844	<5	1.113	3144	4.8 ± 0.8	14.77 ± 0.64	1.32	18
			Zr	20	2.32	1275	4.9	2687	<5	0.433	2165	13.6 ± 1.3	–	–	–
f5	(HB12/97)	TH	Ap	20	0.05	67	2.59	3459	<5	1.02	3176	3.4 ± 0.8	14.0 ± 0.42	1.43	46
			Zr	20	2.15	1820	4.52	3833	<5	0.433	2165	13.7 ± 1.2	–	–	–
f6	(HB5/97)	HHCS	Ap	20	0.008	10	0.493	655	100	1.017	3171	2.7 ± 1.8	–	–	–
f7	(HB6/97)	HHCS	Ap	20	0.02	28	3.91	5470	<5	1.019	3174	0.9 ± 0.4	–	–	–
f8	(HB31/97)	LHCS	Ap	20	0.005	6	1.4	1667	100	1.026	3185	0.7 ± 0.6	–	–	–
			Zr	20	0.252	206	4.22	3457	18	0.433	2165	1.7 ± 0.3	–	–	–
f9	(HB32/97)	LHCS	Zr	20	0.469	217	5.03	2325	94	0.433	2165	2.7 ± 0.4	–	–	–
f10	(HB43/96)	LHCS	Ap	20	0.038	50	3.92	5139	<5	1.028	3187	1.7 ± 0.5	–	–	–
			Zr	11	1.84	255	11	1528	<5	0.433	2165	4.8 ± 0.8	10.75 ± 0.36	1.0	32
f11	(HB66/96)	HHCS	Ap	20	0.022	21	1.29	1237	<5	1.035	3198	3.0 ± 1.4	–	–	–
			Zr	10	2.41	343	5.93	845	5	0.433	2165	11.7 ± 1.7	–	–	–
f12	(HB72/96)	HHCS	Ap	20	0.37	56	2.21	3303	<5	1.037	3201	3.0 ± 0.8	–	–	–
			Zr	20	2.48	1032	6.7	2788	63	0.433	2165	10.7 ± 1.1	–	–	–
f13	(HB52/96)	HHCS	Ap	20	0.02	30	1.08	1616	6	1.029	3189	3.3 ± 1.3	–	–	–
			Zr	20	2.07	1131	5.5	3004	54	0.433	2165	10.8 ± 1.0	–	–	–
f14	(HB59/96)	HHCS	Ap	20	0.019	25	0.881	1127	<5	1.031	3192	4.0 ± 1.7	–	–	–
			Zr	18	2.33	724	5.51	1711	5	0.433	2165	12.2 ± 1.3	–	–	–
f15	(HB63/96)	HHCS	Ap	20	0.024	29	1.04	1254	<5	1.034	3196	4.1 ± 1.6	–	–	–
			Zr	17	1.68	513	3.99	1220	30	0.433	2165	12.1 ± 1.5	–	–	–
f16	(HB61/96)	HHCS	Ap	10	0.038	23	2.01	1227	<5	1.032	3194	3.3 ± 1.5	–	–	–
			Zr	7	3.68	292	9.23	733	15	0.433	2165	11.5 ± 1.7	–	–	–

[a]Original sample number in parentheses.
[b]Mineral analyzed.
[c]Number of crystals analyzed
[d]Track densities (ρ) given as [10^6 tracks cm^{-2}], N = number of tracks; Analyses by external detector method using 0.5 for the $4\pi/2\pi$ geometry correction factor.
[e]$P\chi^2$ is the probability of obtaining χ^2 value for ν degrees of freedom, where ν = number of crystals −1.
[f]Central age; apatite ages calculated using dosimeter glass CN-5 with $\zeta_{CN5} = 343 \pm 5$ (M. Rahn) and 339 ± 5 (A. Carter); zircon ages calculated using dosimeter glass CN-2 with $\zeta_{CN2} = 133 \pm 3$ (M. Rahn).
[g]Mean track length.
[h]Standard deviation of the track length distribution; all uncertainties at 2 sigmas level.

[38] The cooling curve for the HHCS rocks indicates two distinct stages of cooling (Figure 10). Following the metamorphic peak at ~23 Ma, the first stage is characterized by increasing cooling rates (~10 to 60°C/Myr) until circa 16 Ma. This trend reflects an increase of the geothermal gradient as a consequence of heat advection during rapid exhumation [e.g., *Grasemann et al.*, 1998], and the modeled exhumation rate for this stage is ~2.2 mm/yr. This rapid exhumation is consistent with a tectonic extrusion of the HHCS, controlled by coeval thrusting along the MCT and extension along the Sangla Detachment during early Miocene [*Vannay and Grasemann*, 2001]. The second stage of the cooling evolution, between circa 16 and 3 Ma, is marked by a significant decrease of the cooling rates (~60 to 20°C/Myr). This stage is indicative of conductive cooling during slower exhumation of the HHCS, and the modeled exhumation rate for this period is ~0.6 mm/yr. This change strongly suggests that thrusting along the MCT ceased at xaround 16 Ma, and that erosion was the dominant mechanism of exhumation for the HHCS during middle Miocene to Pliocene. This evolution is similar to what is observed in the HHCS of the Bhagirathi Valley, ~70 km to the SE of the Sutlej section (Figure 2), where rapid exhumation controlled by thrusting along the MCT during early Miocene (~23–20 Ma) was followed by slower cooling during middle Miocene to Pliocene (~15–2 Ma), as a consequence of slower exhumation controlled by erosion [*Searle et al.*, 1999]. In the Sutlej section, the cooling rate of the HHCS increased again during the last 3 Myr, indicating enhanced exhumation (modeled exhumation rate = 1 mm/yr) probably related to the exhumation of the LHCS in the MCT footwall. The base of the Tethyan Himalaya cooled between 450 and 290°C ~2–3 Myr earlier compared to the underlying HHCS, indicating a diachronic exhumation of these units due to extension along the Sangla Detachment between early and middle Miocene.

[39] Compared to the MCT hanging wall, the LHCS unit is characterized by a significantly younger and faster cooling history (Figure 10). Thermal modeling suggests a two stages cooling evolution for the LHCS. The first stage,

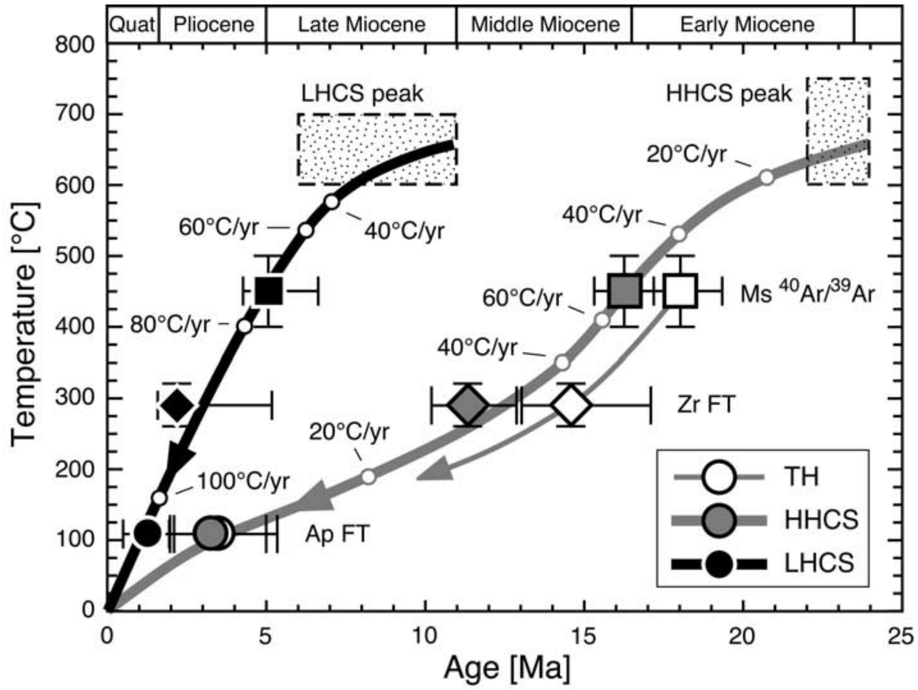

Figure 10. Cooling evolution of the Tethyan Himalaya (TH), HHCS, and LHCS units in the Sutlej section. The symbols correspond to weighted average cooling ages, whereas the horizontal error bars indicate the range of measured ages at 1 sigma level. The cooling curves for the HHCS and LHCS units are deduced from one-dimensional thermal modeling [*Mancktelow and Grasemann*, 1997; *Mancktelow*, 1998], assuming closure temperatures at 450 ± 50°C for Ar diffusion in muscovite, and at 290 ± 30°C and 110 ± 10°C for annealing of fission tracks in zircon and apatite, respectively (see text for more details).

between the metamorphic peak at circa 11–6 Ma down to ~450°C at circa 5 Ma, is characterized by a rapid increase of the cooling rates (~20 to 70°C/Myr) related rapid exhumation at a modeled rate of 3 mm/yr. The second stage, from Pliocene to Quaternary, indicates a slower increase of the cooling rates (~70 to 100°C/Myr) reflecting a decreasing, although still high exhumation rate. The modeled exhumation rate for this stage is 1.8 mm/yr. One zircon sample from the LHCS revealed a narrow fission track length distribution around a mean value of 10.75 μm (sample f10; Table 1), confirming a fast cooling through the zircon partial annealing zone. The rapid exhumation of the LHCS is consistent with a tectonic extrusion controlled by thrusting along the Munsiari Thrust and extension along the Karcham Normal Fault.

[40] The continuously increasing cooling rates indicate that, in contrast to the HHCS, rapid tectonic exhumation of the LHCS continued in shallow structural depths, where the cooling rate reached ~100°C/Myr. As a consequence of rapid heat advection, the modeled near surface geothermal gradient for the LHCS is about 65–70°C/km, in good agreement with actual temperature measurements from an hydro-electric gallery across this unit along the Sutlej Valley (Nathpa-Jhakri Hydel Project; G. Spaun, Technical University Munich, personal communication), as well as with the presence of numerous hydrothermal sources in this unit (Figure 3) [*Srikantia and Bhargava*, 1998]. Our results are thus consistent with the FT data by *Lal et al.* [1999] and *Jain et al.* [2000], indicating a fast Pliocene to Quaternary differential exhumation of the LHCS rocks cropping out in the LKR Window compared to the surrounding HHCS unit.

6. Tectonothermal Evolution

[41] The thermobarometric data discussed above provide information about the burial depth and temperature reached by the units exposed along the Sutlej section, the geochronological data constrain the timing of cooling and exhumation, and the structural analysis constrain the kinematic evolution. These results have been used to reconstruct the Himalayan tectono-thermal evolution along the Sutlej section. This evolution can be subdivided into four main events (Figure 11). It should be noted that the thermal evolution illustrated in Figure 11 is not quantitatively modeled, but designed to be consistent with the available P-T-t constraints.

6.1. Middle Eocene to Early Miocene

[42] The first stage of the tectono-thermal evolution, between middle Eocene and early Miocene, corresponds to underthrusting of Upper Proterozoic to Cambrian sediments of the Indian plate (Figure 11a), gradually metamorphosed into the paragneisses forming the HHCS. This

tectonic event is recorded by the early $D1_H$ ductile deformation observed in the HHCS (Figure 5), as well as by the SW directed thrusting and folding in the overlying Tethyan Himalaya ($D2_T$ phase, Figure 4). A balanced cross section across the Tethyan Himalaya of the Spiti region, ~30 km to the NW of the studied area, indicates that large-scale SW verging deformation in this unit is consistent with thrusting along a major detachment located at the projected level of

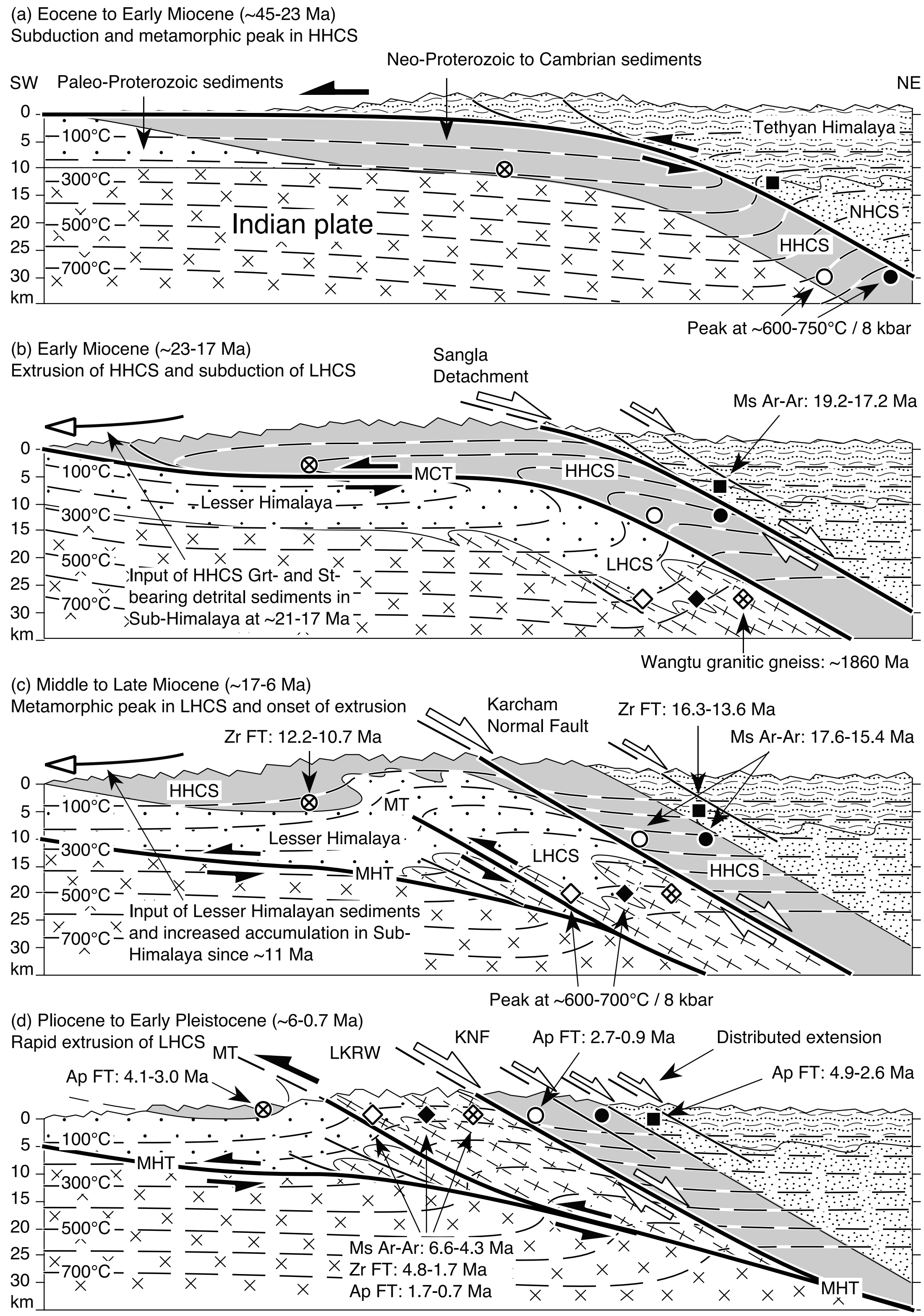

the Sangla Detachment at ∼10 km depth [*Wiesmayr and Grasemann*, 2002]. Moreover, $^{40}Ar/^{39}Ar$ results show that SW verging folding in the Tethyan Himalaya of Spiti occurred during middle Eocene (∼45 and 42 Ma) [*Wiesmayr and Grasemann*, 2002], broadly contemporaneously with underthrusting and prograde metamorphism in the underlying HHCS [*Vance and Harris*, 1999; *Foster et al.*, 2000]. These results indicate that, before being re-activated as an extensional shear zone, the Sangla Detachment initially acted as a thrust beneath which the HHCS was underthrusted. Following the burial of the HHCS, a tectonically inactive period allowed the relaxation of the isotherms bent toward the foreland during underthrusting. This thermal relaxation induced a nearly isobaric heating of the HHCS, and the rocks underthrusted at 30 km depth reached peak temperatures between 600 and 750°C at the onset of early Miocene.

6.2. Early Miocene

[43] The activation of the MCT during early Miocene, since about 23 Ma [*Hubbard and Harrison*, 1989; *Coleman*, 1998; *Catlos et al.*, 2001], triggered exhumation of the HHCS (Figure 11b). In the Sutlej section, the ductile stage of this exhumation is recorded by a second phase of penetrative deformation ($D2_H$), superimposed on, and partly transposing, the earlier structures ($D1_H$) related to the initial underthrusting of the HHCS (Figure 5). Exhumation of the HHCS was also accompanied by extension along the detachments of the STDS at the top of the unit [e.g., *Hodges et al.*, 1992; *Dèzes et al.*, 1999]. In the Sutlej section, the Sangla Detachment at the top of the HHCS most likely reactivated the thrust beneath which the sequence was initially underthrusted beneath the Tethyan Himalaya. A comparable interpretation has been proposed for two others strands of the STDS: the Zanskar Shear Zone and the Annapurna Detachment [*Patel et al.*, 1993; *Vannay and Hodges*, 1996].

[44] The tectonic extrusion of the HHCS induced its rapid exhumation and cooling during early Miocene, as recorded by thermochronological data from the Sutlej (Figure 10), as well as from Zanskar and Garhwal [*Dèzes et al.*, 1999; *Searle et al.*, 1999]. In Zanskar, extrusion of the HHCS was related to an average extensional slip rate in excess of 1.4 cm/yr along the Zanskar Shear Zone, between ∼22 and 20 Ma [*Dèzes et al.*, 1999]. In the Sub-Himalayan foreland basin to the SW and to the west of the studied area, the lower Miocene molasses record an input of detrital garnet and staurolite between about 21 and 17 Ma, the isotopic signature of these sediments indicate that they derive from the HHCS unit, and the detrital muscovite yielded $^{40}Ar/^{39}Ar$ cooling ages just a few Myr older than the depositional age [*Najman and Garzanti*, 2000; *White et al.*, 2002]. These observations confirm a rapid exhumation and erosion of HHCS high-grade metamorphic rocks during early Miocene. At larger scale, this tectonic event is recorded by a sharp increase in accumulation rates during early Miocene in both the Sub-Himalayan foreland basin and the Bengal Fan [*Métivier et al.*, 1999].

[45] While the HHCS was exhumed, Lower Proterozoic sediments of the Indian plate, as well as granitic rocks most likely representing their basement, were underthrusted beneath the MCT (Figure 11b). These rocks were gradually transformed into the paragneiss and orthogneiss now forming the LHCS, as a consequence of underthrusting down to ∼30 km depth, and prograde metamorphism reaching peak temperatures between 600 and 700°C. This underthrusting was responsible for a first phase of penetrative ductile deformation in the LHCS rocks ($D1_L$ phase; Figure 7). In a more frontal part of the orogen, the Lower Proterozoic metasediments and metabasites now forming the Lesser Himalaya reached greenschist facies metamorphic conditions as they were overthrusted by the exhuming HHCS gneiss sheet.

6.3. Middle to Late Miocene

[46] The third main stage of the tectono-thermal evolution of the Sutlej section corresponds to the end of thrusting along the MCT, as well as to the activation of the Munsiari Thrust resulting from the foreland-directed propagation of deformation in the Indian plate (Figure 11c). The decreasing cooling rates recorded by the HHCS in the Sutlej section since ∼16 Ma strongly suggests that the main thrusting movement along the MCT ceased between early to middle Miocene, and that subsequent exhumation was predominantly controlled by erosion (Figure 10).

[47] Beneath the MCT, the LHCS reached metamorphic peak conditions during late Miocene. The subsequent rapid cooling (Figure 10) marks the onset of rapid exhumation associated with thrusting along the Munsiari Thrust and extension along the Karcham Normal Fault at the top of the unit (Figure 11c). The ductile stage of the LHCS extrusion is recorded by a second phase of penetrative deformation in this unit (deformation phase $D2_L$; Figure 7). A late Miocene propagation of thrusting in the MCT footwall is consistent with evidence from the foreland basin. From Pakistan to Nepal, the late Miocene Sub-Himalayan sediments record a pronounced increase in sedimentation rates since about 11 Ma, as well as a renewed input of metamorphic detrital minerals, indicating unroofing of newly exposed metamor-

Figure 11. Cenozoic tectono-thermal evolution of the Himalayan crystalline core zone along the Sutlej section. This semi-quantitative reconstruction is based on the structural and geochronological constraints of the present study, as well as on the P-T results of *Vannay and Grasemann* [1998] and *Vannay et al.* [1999]. The circle, square, and diamond symbols correspond to representative samples (or groups of samples) constraining the underthrusting depth, peak temperature, and chronology of cooling and exhumation of the various units exposed along the section. The evolution of the thermal structure is qualitative and designed to fit the available constraints. Each stage of this reconstruction generally shows the situation toward the end of the time interval illustrated (see text for explanations). Abbreviations are as in Figure 2.

phic terranes in the hinterland [e.g., *Meigs et al.*, 1995; *DeCelles et al.*, 1998; *Métivier et al.*, 1999; *Robinson et al.*, 2001]. In Nepal, more than 400 km to the SE of the Sutlej, sedimentological and neodymium isotopic results indicate that, although the Eocene to Pliocene Sub-Himalayan deposits mainly record the erosion of the HHCS and Tethyan Himalaya, a marked shift occurring at ~11–10 Ma testifies of an increasing detrital input from Lesser Himalaya rocks [*DeCelles et al.*, 1998; *Robinson et al.*, 2001]. This change is interpreted as reflecting the erosional breaching of Lesser Himalayan units through the HHCS rocks previously overthrusted onto them, as a consequence of thrusting in the footwall of the MCT [*DeCelles et al.*, 1998; *Robinson et al.*, 2001]. At the larger scale, the post-MCT renewed phase of thrusting and exhumation at the Himalayan front since late Miocene is temporally correlated with an abrupt increase in accumulation rates of terrigenous sediments in the northern Indian Ocean since ~11 Ma [*Rea*, 1992].

6.4. Pliocene to Pleistocene

[48] The final stage of the tectono-metamorphic evolution, between Pliocene to late Pleistocene, corresponds to the rapid exhumation and cooling of the LHCS (Figures 10 and 11d). This late exhumation was associated with an increasingly brittle faulting along the Munsiari Thrust and Karcham Normal Fault, as well as along numerous minor extensional structures distributed in the hanging wall of the MCT (Figure 3). Thrusting of the LHCS along the Munsiari Thrust induced the development of a large-scale fault-related antiform, that eventually resulted in creation of the Larji-Kulu-Rampur tectonic window, as the LHCS finally breached through the overlying HHCS rocks previously overthrusted along the MCT (Figures 2 and 11d).

7. Active Tectonics

[49] Several observations demonstrate that tectonic extrusion of the LHCS continued during Holocene, and that it is still active: (1) in good agreement with thermochronological results indicating high cooling rates in excess of 100°C/Myr during the past ~2 Myr (Figure 10), the LHCS is still characterized by high near-surface geothermal gradients, as revealed by the presence of several hot springs in this unit (Figure 3), as well as by temperature measurements in the hydro-electric gallery of the Nathpa-Jhakri Project (G. Spaun, personal communication); (2) syn-sedimentary extension in the hanging wall of the MCT is recorded within Holocene intra-mountain lake deposits from the Baspa Valley (Figure 6d) [*Draganits et al.*, 2001]; (3) neo-tectonic and seismic results indicate active tectonic uplift in the Larji-Kulu-Rampur Window [*Dubey et al.*, 2003]; and (4) the present-day seismic data indicates that SW directed thrusting is still going on at the level of the Munsiari Thrust in Garhwal (e.g., 1991 Uttarkashi earthquake) [*Kayal*, 1996], whereas east directed extension is taking place in the MCT hanging wall in the Sutlej region (Figure 2) [*Molnar and Lyon-Caen*, 1989]. This contrasting strain regime across the MCT is strikingly similar to the one revealed by the brittle-ductile to brittle structures along the Sutlej section (Figure 3), and it is consistent with ongoing tectonic extrusion of the LHCS along the Munsiari Thrust.

8. Vigorous Fluvial Erosion Along the Sutlej

[50] The rapid exhumation of the LHCS unit since late Miocene, as well as the previous exhumation of the HHCS since early Miocene, imply that a significant volume of rock must have been removed by erosion along the Sutlej Valley (Figure 11). Quantitative results about erosion along the Sutlej Valley are still limited, despite the fact that landslides, flash floods, soil erosion, and rapid siltation of dam reservoir represent major consequences of rapid erosion in this region [*Sharma et al.*, 1991]. A quantitative analysis of erosion patterns and sediment transport in this area is currently under way [e.g., *Bookhagen et al.*, 2003], but several observations already indicate vigorous erosion along the Sutlej River. Although originating from the same region as the Indus and the Tsangpo-Brahmaputra (Figure 1), the Sutlej takes a more direct course toward the Indian Ocean, and it is the third largest river entirely crosscutting the Himalayan range (Figure 12). The Sutlej is thus generally interpreted as being antecedent to the uplift of the Himalaya [*Seeber and Gornitz*, 1983], although it cannot be ruled out that it evolved by regressive erosion across the range, to eventually capture a north Himalayan drainage [*Brookfield*, 1998]. Both scenarios imply that strong fluvial erosion allowed the Sutlej to maintain, or carve, its course across the uplifting Himalaya.

[51] Like the Indus and the Tsangpo-Brahmaputra, the Sutlej cuts deep gorges through the crystalline units of the High Himalaya. Across the HHCS and LHCS units, the Sutlej Valley is ~20 to 30 km wide, with a topographic relief reaching up to about 5 km (Figure 12b). In this region forming the hanging wall of the Munsiari Thrust, the Sutlej's longitudinal profile is characterized by steep gradients, significantly exceeding the ideal profile slope (Figure 12c). In good agreement with the thermochronological results of the present study, this feature confirms the active tectonic uplift of the hanging wall of the Munsiari Thrust [*Seeber and Gornitz*, 1983]. This part of the Sutlej Valley, west of the High Himalayan rainfall barrier, is also characterized by a very humid climate. Mean precipitations of ~3 m/yr, combined with steep topographic slopes, result in active erosion through hillslope processes [*Bookhagen et al.*, 2003]. During the monsoon season, major landslides, sometimes triggered by seismic activity (e.g., 1975 Kinnaur earthquake), regularly occur along the Sutlej Valley. The erosional potential of the Sutlej is occasionally illustrated by catastrophic flash floods. In August of 2000, for example, a major flood originating in Tibet caused significant loss of life and material damage along a 270 km long stretch of the Sutlej Valley, as the water level rose up to 12 m above normal level in the narrowest gorges (Figure 13). Sudden floods, resulting from heavy rain or failure of natural dams, appear to be a regular phenomenon in the Sutlej Valley (e.g., 1997 and 1988), and such floods must significantly contribute to the removal of eroded rocks out of the valley.

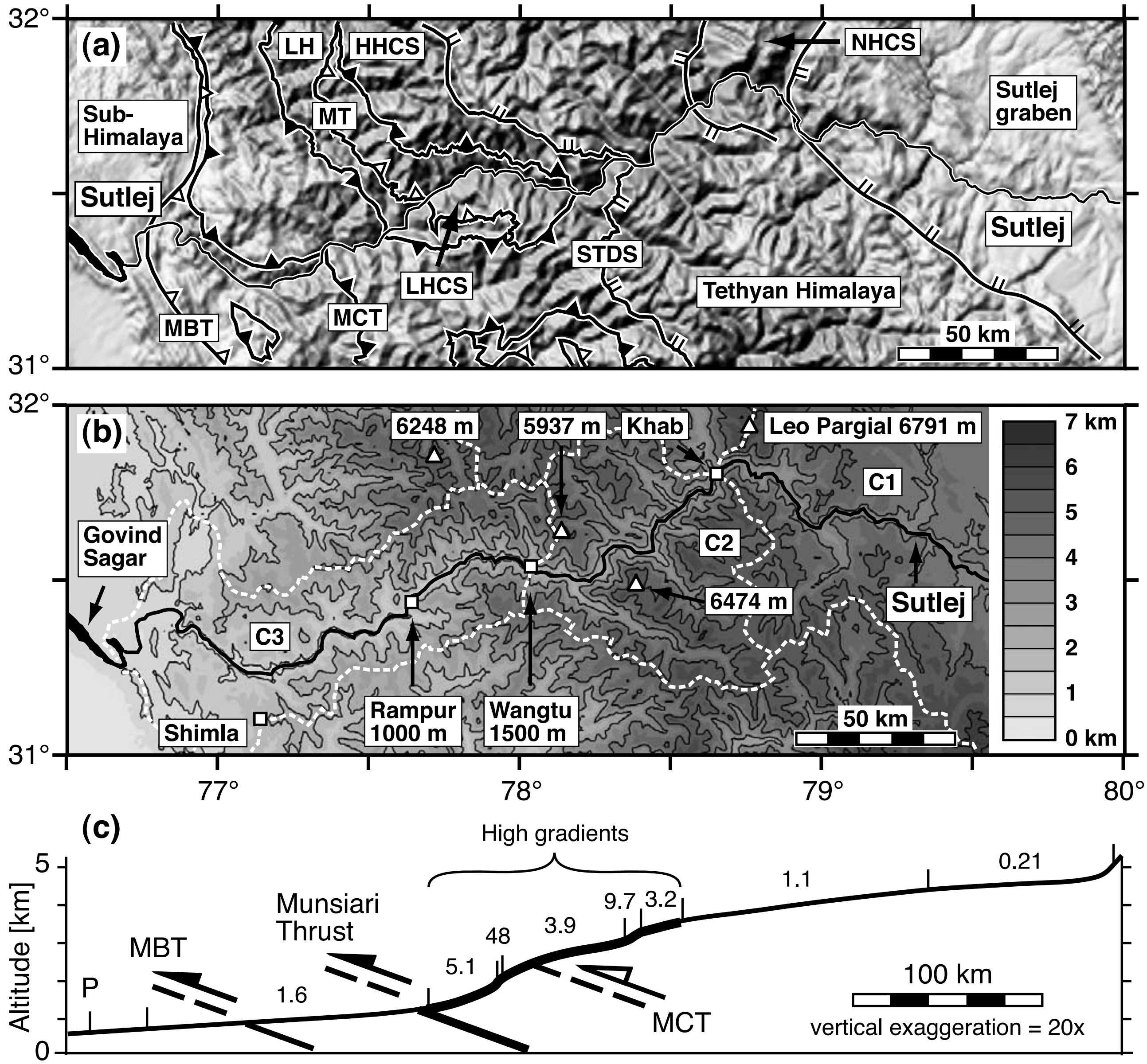

Figure 12. Geomorphic features of the Sutlej Valley in the NW Himalaya. (a) Shaded relief map with major tectonic contacts (abbreviations are as in Figure 2). (b) Elevation map with 1 km contour lines (topographic data: GTOPO30, U.S. Geological Survey). The dashed open lines delimit the drainage area of the Sutlej River, subdivided into three sub-catchments (C1 to C3). On the basis of sediment load measurements from the Sutlej at Khab, Wangtu, and Govind Sagar reservoir [*Sharma et al.*, 1991], integrated average erosion rates are 0.14 mm/yr in the Tibetan part of the Sutlej (C1), 1.6 mm/yr in Kinnaur (C2), and 1.8 mm/yr in the frontal part of the Himalaya (C3). (c) Vertically exaggerated longitudinal profile of the Sutlej river [after *Seeber and Gornitz*, 1983]. The numbers between tick marks along the profile correspond the ratio of the actual stream gradient index (slope multiplied by distance to source) to the gradient index of an idealized graded Sutlej river following a semi-logarithmic profile. The thicker segment along the profile indicates actual stream gradient indexes more than twice the value for the equilibrium profile. The tick mark labeled "P" indicates the entrance of the Sutlej in the Indian plain.

[52] On the basis of topographic and precipitation data, and using models of bedrock river incision, a rate-of-erosion index (erosion rate divided by erodibility) has been calculated for the entire Himalayan range by *Finlayson et al.* [2002]. This work indicates that both the Indus and Tsangpo-Brahmaputra rivers are characterized by high erosion indexes at the level of the Nanga Parbat and Namche Barwa syntaxes. High erosion indexes are unlikely to reflect low coefficients of erosion in these regions predominantly composed of resistant crystalline rocks, and they confirm

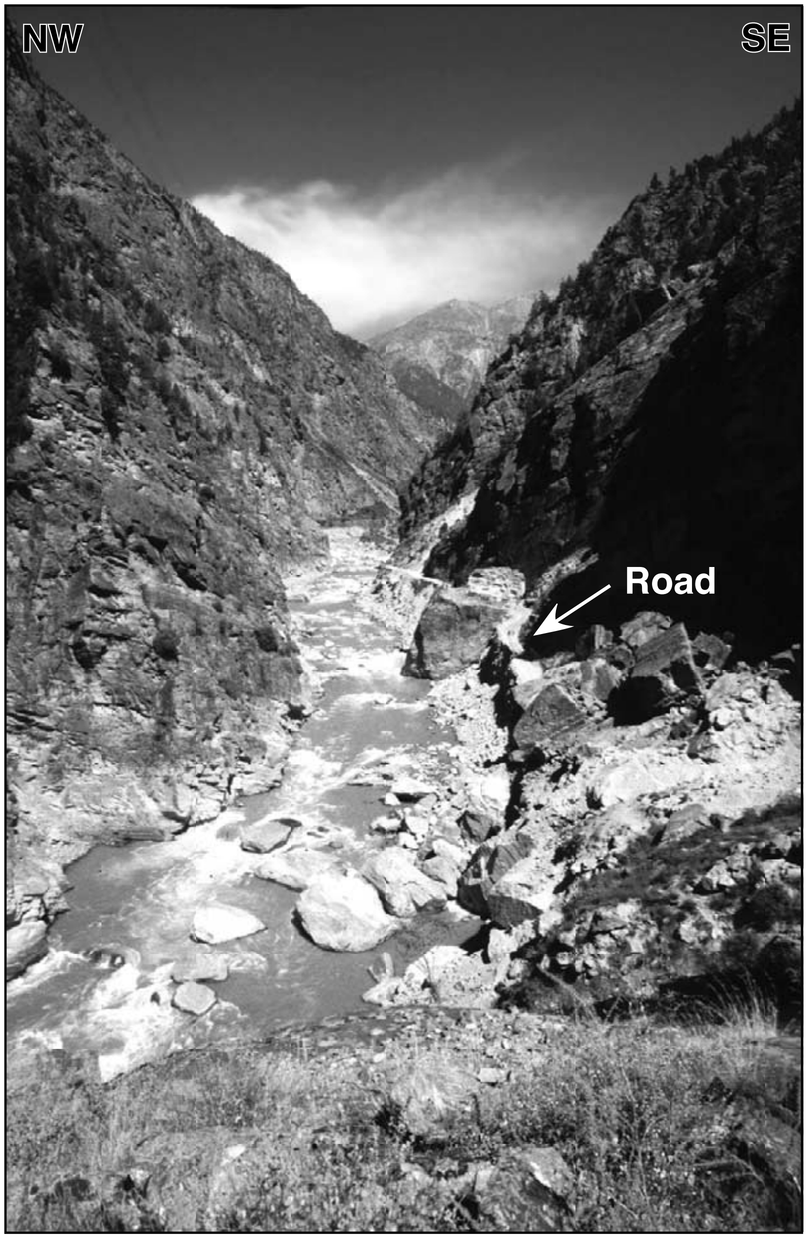

Figure 13. Gorges cut by the Sutlej across the HHCS paragneisses (between Karcham and Peo). Note the spectacular rockfall caused by a major flash flood on 1 August 2000. The larger blocks have decametric size (road for scale).

that the Himalayan syntaxes correspond to localized zones of high erosion potential, in good agreement with field-based results [e.g., *Zeitler et al.*, 2001]. Interestingly, the area of the Sutlej Valley is also characterized by a high fluvial erosion index, and it appears to correspond to one of the main zones of focused high erosional potential between the syntaxes (Figure 2) [*Finlayson et al.*, 2002].

[53] General estimates of present-day erosion rates in the Sutlej area can be derived from measurements of sediment loads and catchments areas [*Sharma et al.*, 1991]. In the foothills of the most frontal part of the Himalaya, the Govind Sagar reservoir created by the Bhakra hydroelectric dam (Figure 12b) has a total catchment area of $\sim$56,860 km^2, corresponding to the entire upstream drainage area of the Sutlej River (including the Spiti River). This reservoir is being rapidly silted as a consequence of an annual sedimentation load about 35,800,000 m^3/yr [*Sharma et al.*, 1991], implying an integrated average erosion rate $\sim$0.6 mm/yr over the entire Himalayan catchment of the Sutlej. Estimates of integrated average erosion rates for sub-catchments indicate, however, limited erosion in the Tibetan part of the Sutlej ($\sim$0.14 mm/yr), and increasing erosion rates in the High Himalayan range (1.6 mm/yr, Figure 12b).

[54] In the frontal part of the Sutlej's Himalayan catchment, downstream from Wangtu, the average erosion rate is ~1.8 mm/yr. This estimate probably represents a minimum value for erosion in the exhuming LHCS unit, because erosion rates in the Himalayan foothills (Lesser Himalaya and Sub-Himalaya) are most likely lower than in the topographically steeper Himalayan range, as predicted by the erosion index maps by *Finlayson et al.* [2002]. The average erosion rate for the frontal part of the range is consequently consistent with the Pliocene to present-day exhumation rate for the LHCS unit (1.8 mm/yr) deduced from modeling of the thermochronological data, although the uncertainties (not quantified) associated with these estimates must be kept in mind. Estimates of erosion rates in the Sutlej appears nevertheless to be broadly consistent with what is observed along the Upper Ganges catchment (Bhagirathi and Alaknanda valleys, Figure 2), where cosmogenic isotopes constrain an average erosion rate of 2.7 ± 0.3 mm/yr in the High Himalayan range, whereas erosion rates in the foothills are 0.8 ± 0.3 to lower than 0.6 mm/yr [*Vance et al.*, 2003].

9. Feedback Between Tectonics and Erosion

[55] Like the Sutlej, the Indus and the Tsangpo-Brahmaputra originate north of the Himalayan range, in the vicinity of Mount Kailash, ~300 km to the east of the studied area (Figure 1). In contrast to the Sutlej, however, the Indus and the Tsangpo-Brahmaputra both flow around the entire Himalayan barrier, to the NW and to the east, respectively, to finally crosscut the range at the level of the Nanga Parbat and Namche Barwa syntaxial extremities of the belt. Both of these syntaxes correspond to very active continental tectonic settings, characterized by exposure of Pliocene to Pleistocene, high temperature metamorphic rocks and granitic intrusions, high geothermal gradients, extreme topographic gradients, and some of the highest exhumation and fluvial incision rates measured on the Earth [e.g., *Burg et al.*, 1997; *Shroder and Bishop*, 2000; *Zeitler et al.*, 2001].

[56] This close spatial coincidence between active exhumation of deep crustal rocks and vigorous fluvial erosion strongly suggests that geomorphic processes can have a major influence on the tectono-thermal evolution of orogens, such as predicted by numerical modeling [e.g., *Jamieson and Beaumont*, 1989; *Beaumont et al.*, 1992; *Koons*, 1995; *Koons et al.*, 2002]. Through rapid fluvial incision and efficient removal of erosional sediments from the uplifted region, major trans-orogenic rivers, such as the Indus and the Tsangpo-Brahmaputra, most likely amplify isostatic and tectonic uplift, leading in turn to enhancing heat advection and contributing to further rheological weakening of the crust. Such a positive feedback between focused erosion and enhanced crustal reworking has been dubbed a "tectonic aneurysm" by *Zeitler et al.* [2001], in the sense of self-sustained failure of a normally strong boundary.

[57] The geological evolution of the Sutlej section shares several significant similarities with what is observed in the Nanga Parbat syntaxis: (1) a late Miocene to present-day rapid exhumation of high-grade metamorphic rocks derived from Lesser Himalayan protoliths, and resulting in the creation of a large-scale tectonic window (Figures 10 and 11); (2) several hydrothermal springs that testify, consistently with thermochronology results, to elevated near-surface geothermal gradients due to heat advection during rapid exhumation of the LHCS unit (Figure 3); and (3) the presence of a major trans-Himalayan river characterized by a strong erosion potential, and creating a significant topographic gap across the orogen (Figure 12). The Sutlej section is consequently characterized by a close spatial correlation between vigorous erosion and late Neogene to present-day rapid exhumation of deep crustal rocks, such as observed in the "tectonic aneurysm" contexts of the Himalayan syntaxes.

[58] Thermo-mechanical numerical modeling by *Koons et al.* [2002] confirms that focused fluvial incision at the scale of large river gorges, such as in the Nanga Parbat Massif, can result in concentration of strain in topographic gaps, where localized advection of deep crustal rocks can occur as a consequence of efficient erosional removal of material. As a consequence of heat advection, thermal thinning of the upper brittle crust induces the creation of a rheological weak spot, where exhumation becomes increasingly concentrated due to a positive feedback between thermal weakening and erosion-controlled strain concentration. *Koons et al.* [2002] conclude that in order to have a significant influence on collisional strain pattern, fluvial erosion must be: (1) sufficient to create and maintain a significant transverse topographic gap across the belt, with a width at least as great as the thickness of the upper, high strength brittle layer of the crust (~15 km); and (2) the topographic gap must be initiated near a major thrust where the region is already close to failure. The Sutlej region appears to satisfy both criteria given that: (1) the Sutlej Valley is approximately 20 to 30 km wide, with a topographic relief that can reach up to ~5 km; (2) the Sutlej river must induce incision rates sufficient to maintain its course across the actively uplifting range; and (3) the Sutlej river cuts deep gorges through crystalline units both bounded by major thrusts at their base.

[59] These features, together with the results of the present study, strongly suggest that active tectonic exhumation and fluvial erosion are coupled along the Sutlej River. The Kishtwar tectonic window along the Chenab Valley, ~260 km to the NW of the Sutlej section, appears to represent another example of a spatial correlation between fluvial erosion and late Neogene to still active exhumation of deep crustal rocks within a crustal-scale antiformal tectonic window between the syntaxes. Like the LKW Window discussed in this study, the Kishtwar Window corresponds to a large-scale antiformal structure exposing Lesser Himalayan rocks through the HHCS gneisses previously overthrusted along the MCT. The Lesser Himalayan rocks of the Kishtwar window yielded Pliocene to Holocene fission track cooling ages, demonstrating a young and rapid differential exhumation compared to the overlying HHCS [*Kumar et al.*, 1995]. Interestingly, the erosion index map calculated by *Finlayson et al.* [2002] points out that the area surrounding the Chenab river where it crosses the Kishtwar window corresponds to the main anomalous zone of high

erosional potential between the Sutlej Valley and the Nanga Parbat massif.

[60] A geomorphic influence on crustal-scale processes is consequently not necessarily restricted to the Himalayan syntaxes, although these regions probably represent extreme examples of "tectonic aneurysms" because of focused strain at the edges of the Indian plate indenter and intense fluvial erosion along the two mightiest Trans-Himalayan rivers. Evidence for active tectonics coupled to focused erosion in the Sutlej Valley, and also probably along the Chenab Valley, provide additional field-based arguments supporting the emerging view of a positive feedback interaction between surficial processes and the tectono-thermal evolution of an orogen [e.g., *Zeitler et al.*, 2001; *Koons et al.*, 2002; *Finlayson et al.*, 2002]. Additionally, these results are consistent with numerical modeling predicting that focused erosion at the Himalayan front most likely exerted a first-order control on the thermo-mechanical evolution along the entire range [*Beaumont et al.*, 2001].

10. Conclusions

[61] The new structural and geochronological results presented in this study demonstrate that the crystalline core zone of the Himalayan orogen exposed along the Sutlej Valley is composed of two distinct units, characterized by chronologically contrasting tectono-thermal evolutions controlled by major thrusts. The HHCS represents part of the Neo-Proterozoic to Cambrian sedimentary cover of the Indian plate, underthrusted and metamorphosed up to partial melting conditions between the Eocene and early Miocene. Initial exhumation of this unit was controlled by combined thrusting along the MCT and extension along faults of the South Tibetan Detachment System during early Miocene, whereas erosion took over as the main exhumation mechanism from the middle Miocene. Underthrusting of Paleo-Proterozoic sediments and granitic basement rocks in the footwall of the MCT led to the creation of a second high-grade metamorphic unit. This LHCS crystalline sheet was rapidly exhumed and cooled between late Miocene and Pliocene, as a consequence of thrusting along the Munsiari Thrust and extension in the MCT hanging wall. The kinematic evolution along the Sutlej section indicates that crustal shortening in the active, frontal part of the Himalayan orogen is accommodated by a cyclic succession of continental underthrusting, followed by thrusting and exhumation of high-grade rocks due to the foreland-directed propagation of deformation in the Indian plate margin.

[62] Evidence for Holocene tectonic activity in the Sutlej Valley, as well as the seismicity in the adjacent Garhwal region, indicate that the Munsiari Thrust is still active, and that it most likely represents one of the main intracrustal faults accommodating some of the present-day 1 to 2 cm/yr of convergence across the Himalaya. Active exhumation of deep crustal rocks in the hanging wall of the Munsiari Thrust is spatially correlated with the strong erosional potential of the Sutlej River [*Finlayson et al.*, 2002], suggesting a positive feedback relationship between the deep tectono-thermal evolution and surficial processes [*Beaumont et al.*, 1992; *Zeitler et al.*, 2001; *Koons et al.*, 2002]. Examples of recent to contemporary spatial correlation between efficient erosion and active tectonics, such as in the Himalaya or the Southern Alps of New Zealand, only provide circumstantial evidence for a strong positive interaction between these processes [*Beaumont et al.*, 1992; *Koons*, 1995; *Zeitler et al.*, 2001, and references therein]. As noted by *Beaumont et al.* [1992], paleo-climatic information are most likely required to fully appreciate the influence of erosion on the evolution of ancient orogens. It is therefore interesting to note that the post-MCT renewed tectonic activity at the Himalayan front since late Miocene (Figure 11) [*DeCelles et al.*, 1998; *Robinson et al.*, 2001] is broadly coeval with intensification of the Asian monsoon since about 9–8 Ma [e.g., *Prell et al.*, 1992]. The increase in seasonal discharge associated with the monsoon is likely to have significantly accelerated erosion in the Himalaya, as recorded by a major increase in fluvial channel size at ~10.8 Ma in the Sub-Himalaya [*DeCelles et al.*, 1998], as well as by the increased sediment accumulation rates in both the Sub-Himalayan foreland basin and in the northern Indian Ocean since about 11 Ma [*Meigs et al.*, 1995; *Rea*, 1992; *Métivier et al.*, 1999]. A positive interaction between active tectonics, increased rainfall, and rapid erosion at the frontal part of the Himalayan orogen is thus likely to have persisted from late Miocene to present-day, and the associated enhanced weathering may have had a significant impact on the late Neogene global climatic change [e.g., *Filippelli*, 1997; *Ruddiman et al.*, 1997].

[63] **Acknowledgments.** We are grateful to B. Bookhagen, E. Catlos, E. Draganits, M.-L. Filippi, M. Girard, C. Hager, C. Janda, M. Robyr, M. Schlup, A. Steck, M. Strecker, and R. Thiede, for providing unpublished data, assisting with field work, and fruitful discussions. We thank J.-P. Burg, M. Ducea, and P. Zeitler for critical and constructive reviews that significantly improved the manuscript. J.-C. Vannay and B. Grasemann acknowledge financial support from the Swiss National Science Foundation (FNS grant 2000-058777.99), and from the Austrian Science Fund (grants P-14129-GEO and P-13227-GEO), respectively.

References

Ahmad, T., N. Harris, M. Bickle, H. Chapman, J. Bunbury, and C. Prince (2000), Isotopic constraints on the structural relationships between the Lesser Himalayan Series and the High Himalayan Crystalline Series, Garhwal Himalaya, *Geol. Soc. Am. Bull.*, *112*, 467–477.

Beaumont, C., P. Fullsack, and J. Hamilton (1992), Erosional control of active compressional orogens, in *Thrust Tectonics*, edited by K. R. McClay, pp. 1–18, Chapman and Hall, New York.

Beaumont, C., R. A. Jamieson, M. H. Nguyen, and B. Lee (2001), Himalayan tectonics explained by extrusion of a low-viscosity crustal channel coupled to focused surface denudation, *Nature*, *414*, 738–742.

Bookhagen, B., R. C. Thiede, and M. R. Strecker (2003), Mass movements, erosion patterns and sediment transport along the Sutlej River (NW-Himalaya), *Geophys. Res. Abstr.*, 5Abstract EAE03-A-04043.

Brookfield, M. E. (1998), The evolution of the great river systems of southern Asia during the Cenozoic India-Asia collision: Rivers draining southward, *Geomorphology*, *22*, 285–312.

Burbank, D. W., L. Leland, E. Fielding, R. S. Anderson, N. Brozovic, M. R. Reid, and C. Duncan (1996), Bedrock incision, rock uplift and threshold hillslopes in the northwestern Himalaya, *Nature*, *379*, 505–510.

Burchfiel, B. C., Z. Chen, K. V. Hodges, Y. Liu, L. H. Royden, C. Deng, J. Xu (1992), The South Tibetan detachment system, Himalayan Orogen: Extension contemporaneous with and parallel to shortening in a collisional mountain belt, *Spec. Pap. Geol. Soc. Am.*, *269*, 41 pp.

Burg, J. P., P. Davy, P. Nievergelt, F. Oberli, D. Seward, Z. Diao, and M. Meier (1997), Exhumation during crustal folding in the Namche Barwa syntaxis, *Terra Nova*, *9*, 117–123.

Burghele, A. (1987), Propagation of error and choice of standard in the $^{40}Ar/^{39}Ar$ technique, *Chem. Geol.*, *66*, 17–19.

Burtner, R., A. Nigrini, and R. A. Donelick (1994), Thermochronology of Lower Cretaceous source rocks in the Idaho-Wyoming thrust belt, *AAPG Bull.*, *78*, 1613–1636.

Catlos, E. J., T. M. Harrison, M. J. Kohn, M. Grove, F. J. Ryerson, C. E. Manning, and B. N. Upreti (2001), Geochronologic and thermobarometric constraints on the evolution of the Main Central Thrust, central Nepal Himalaya, *J. Geophys. Res.*, *106*, 16,177–16,204.

Coleman, M. E. (1998), U-Pb constraints on Oligocene-Miocene deformation and anatexis within the Central Himalaya, Marsyandi valley, Nepal, *Am. Sci. J.*, *298*, 553–571.

Cosca, M. A., K. Mezger, and E. J. Essene (1998), The Baltica-Laurentia connection: Sveconorwegian (Grenvillian) metamorphism, cooling, and unroofing in the Bamble Sector, *J. Geol.*, *106*, 539–552.

Dalrymple, G. B., E. C. Alexander Jr., M. A. Lanphere, and G. P. Kraker (1981), Irradiation of samples for $^{40}Ar/^{39}Ar$ dating using the Geological Survey TRIGA reactor, *U.S. Geol. Surv. Prof. Pap.*, *1176*, 55 pp.

DeCelles, P. G., G. E. Gehrels, J. Quade, T. P. Ojha, P. A. Kapp, and B. N. Upreti (1998), Neogene foreland basin deposits, erosional unroofing, and the kinematic history of the Himalayan fold-thrust belt, western Nepal, *Geol. Soc. Am. Bull.*, *110*, 2–21.

DeCelles, P. G., G. E. Gehrels, J. Quade, B. LaReau, and M. Spurlin (2000), Tectonic implications of U-Pb zircon ages of the Himalayan orogenic belt in Nepal, *Science*, *288*, 497–499.

Dèzes, P. J., J.-C. Vannay, A. Steck, F. Bussy, and M. Cosca (1999), Synorogenic extension: Quantitative constraints on the age and displacement of the Zanskar Shear Zone (northwest Himalaya), *Geol. Soc. Am. Bull.*, *111*, 364–374.

Draganits, E., B. Bookhagen, S. Gier, B. Grasemann, C. C. Hofmann, C. Janda, and C. Hager (2001), Deformation structures in rockfall-dammed lake sediments near Sangla: Implications on neotectonic activity in the Sutlej region (NW India), *J. Asian Earth Sci.*, *1*, 14.

Dubey, C. S., G. D. Gupta, B. K. Sharma, E. J. Catlos (2003), Seismicity, related neotectonic activity, uplift and erosion of Lesser Himalaya in between MCT and MBT: Signature of detachment thrust, paper presented at the 18th Himalaya-Karakoram-Tibet Workshop, Eidg. Tech. Hochsch. (ETH) Zürich, Ascona, Switzerland.

Filippelli, G. M. (1997), Intensification of the Asian monsoon and chemical weathering event in the late Miocene-early Pliocene: Implications for late Neogene climatic change, *Geology*, *25*, 27–30.

Finlayson, D. P., D. R. Montgomery, and B. Hallet (2002), Spatial coincidence of rapid inferred erosion with young metamorphic massifs in the Himalayas, *Geology*, *30*, 219–222.

Foster, G., P. Kinny, D. Vance, C. Prince, and N. Harris (2000), The significance of monazite U-Th-Pb age data in metamorphic assemblages: A combined study of monazite and garnet chronometry, *Earth Planet. Sci. Lett.*, *181*, 327–340.

Frank, W., B. Grasemann, P. Guntli, and C. Miller (1995), Geological map of the Kishtwar-Chamba-Kulu region (NW Himalaya India), *Jahrb. Geol. Bundesanst.*, *138*, 299–308.

Frimmel, H. E., and W. Frank (1998), Neoproterozoic tectono-thermal evolution of the Gariep Belt and its basement, Namibia and South Africa, *Precambrian Res.*, *90*, 1–28.

Grasemann, B., L. Ratschbacher, and B. R. Hacker (1998), Exhumation of ultrahigh-pressure rocks: Thermal boundary conditions and cooling history, in *When Continents Collide, Geodynamics and Geochemistry of Ultrahigh-Pressure Rocks*, edited by B. R. Hacker and J. G. Liou, pp. 117–139, Kluwer Acad., Norwell, Mass.

Grasemann, B., H. Fritz, and J.-C. Vannay (1999), Quantitative kinematic flow analysis from the Main Central Thrust Zone (NW-Himalaya, India): Implications for a decelerating strain path and the extrusion of orogenic wedges, *J. Struct. Geol.*, *21*, 837–853.

Grasemann, B., K. Stüwe, and J.-C. Vannay (2003), Sense and non-sense of shear in flanking structures, *J. Struct. Geol.*, *25*, 19–34.

Harrison, T. M., M. Grove, M. Lovera, and E. J. Catlos (1998), A model for the origin of Himalayan anatexis and inverted metamorphism, *J. Geophys. Res.*, *103*, 27,017–27,032.

Hodges, K. V. (2000), Tectonics of the Himalaya and southern Tibet from two perspectives, *Geol. Soc. Am. Bull.*, *112*, 324–350.

Hodges, K. V., R. R. Parrish, T. B. Housh, D. R. Lux, B. C. Burchfiel, L. H. Royden, and Z. Chen (1992), Simultaneous Miocene extension and shortening in the Himalayan orogen, *Science*, *258*, 1466–1469.

Hubbard, M. S., and T. M. Harrison (1989), $^{40}Ar/^{39}Ar$ age constraints on deformation and metamorphism in the MCT zone and Tibetan slab, eastern Nepal Himalaya, *Tectonics*, *8*, 865–880.

Hurford, A. J., and P. F. Green (1983), The Zeta age calibration of fission-track dating, *Chem. Geol.*, *41*, 285–317.

Jain, A. K., D. Kumar, S. Singh, A. Kumar, and N. Lal (2000), Timing, quantification and tectonic modelling of Pliocene-Quaternary movements in the NW Himalaya: Evidence from fission track dating, *Earth Planet. Sci. Lett.*, *179*, 437–451.

Jamieson, R. A., and C. Beaumont (1989), Deformation and metamorphism in convergent orogens: A model for uplift and exhumation of metamorphic terrains, in *Evolution of Metamorphic Belts*, edited by J. S. Daly, R. A. Cliff, and B. W. D. Yardley, *Geol. Soc. Spec. Publ.*, *43*, 117–129.

Janda, C., C. Hager, B. Grasemann, E. Draganits, J.-C. Vannay, B. Bookhagen, and R. Thiede (2002), The Karcham Normal Fault: Implications for an active extruding wedge, Sutlej Valley, NW Himalaya, *J. Asian Earth Sci.*, *20*, 19–20.

Kayal, J. R. (1996), Precursor seismicity, foreshockx and aftershocks of the Uttarkashi earthquake of October 20, 1991 at Garhwal Himalaya, *Tectonophysics*, *263*, 339–345.

Kirschner, D. L., M. A. Cosca, J. C. Hunziker, and H. Masson (1996), Staircase $^{40}Ar/^{39}Ar$ spectra of fine-grained white mica: Timing and duration of deformation and empirical constraints on argon diffusion, *Geology*, *24*, 747–750.

Koons, P. O. (1995), Modeling the topographic evolution of collisional belts, *Annu. Rev. Earth Planet. Sci.*, *23*, 375–408.

Koons, P. O., P. K. Zeitler, C. P. Chamberlain, D. Craw, and A. S. Meltzer (2002), Mechanical links between erosion and metamorphism in Nanga Parbat, Pakistan Himalaya, *Am. J. Sci.*, *302*, 749–773.

Kumar, A., N. Lal, A. K. Jain, and R. B. Sorkhabi (1995), Late Cenozoic-Quaternary thermo-tectonic history of Higher Himalayan Crystalline (HHC) in Kishtwar-Padar-Zanskar region: Evidence from fission track ages, *J. Geol. Soc. India*, *45*, 375–391.

Kwatra, S. K., S. Singh, V. P. Singh, R. K. Sharma, B. Rai, and N. Kishor (1999), Geochemical and geochronological characteristics of the Early Paleozoic granitoids from Sutlej-Bapsa Valleys, Himachal Himalaya, in *Geodynamics of the NW Himalaya*, edited by A. K. Jain and R. M. Manickavasagam, *Gondwana Res. Group Mem.*, *6*, pp. 144–158.

Lal, N., Y. P. Mehta, D. Kumar, A. Kumar, and A. K. Jain (1999), Cooling and exhumation history of the Mandi granite and adjoining tectonic units, Himachal Pradesh, and estimation of closure temperature from external surface of zircon, in *Geodynamics of the NW Himalaya*, edited by A. K. Jain and R. M. Manickavasagam, *Gondwana Res. Group Mem.*, *6*, Japan, 207–216.

Mahajan, A. K., and N. S. Virdi (2001), Macroseismic field generated by 29 March, 1999 Chamoli Earthquake and its seismotectonics, *J. Asian Earth Sci.*, *19*, 507–516.

Mancktelow, N. S. (1998), A stepwise discrete Fourier transform approach to 1-D thermal modelling of exhumation by erosion and stretching, *Comput. Geosci.*, *24*, 829–837.

Mancktelow, N., and B. Grasemann (1997), Time-dependent effects of heat advection and topography on cooling histories during erosion, *Tectonophysics*, *270*, 167–195.

Meigs, A. J., D. W. Burbank, and R. A. Beck (1995), Middle-late Miocene (>10 Ma) formation of the Main Boundary thrust in the western Himalaya, *Geology*, *23*, 423–426.

Metcalfe, R. P. (1993), Pressure, temperature and time constraints on metamorphism across the Main Central Thrust zone and High Himalayan Slab in the Garhwal Himalaya, in *Himalayan Tectonics*, edited by P. J. Treloar and M. P. Searle, *Geol. Soc. Spec. Publ.*, *74*, 485–509.

Métivier, F., Y. Gaudemer, P. Tapponnier, and M. Klein (1999), Mass accumulation rates in Asia during the Cenozoic, *J. Geophys. Int.*, *137*, 280–318.

Miller, C., U. Klötzli, W. Frank, M. Thöni, and B. Grasemann (2000), Proterozoic crustal evolution in the NW Himalaya (India) as recorded by circa 1.80 Ga mafic and 1.84 Ga granitic magmatism, *Precambrian Res.*, *103*, 191–206.

Molnar, P., and H. Lyon-Caen (1989), Fault plane solutions of earthquakes and active tectonics of the Tibetan Plateau and its margins, *J. Geophys. Int.*, *99*, 123–153.

Najman, J., and E. Garzanti (2000), Reconstructing early Himalayan tectonic evolution and paleogeography from Tertiary foreland basin sedimentary rocks, northern India, *Geol. Soc. Am. Bull.*, *112*, 435–449.

Ni, J., and M. Barazangi (1984), Seismotectonics of the Himalayan collision zone: Geometry of the underthrusting Indian plate beneath the Himalaya, *J. Geophys. Res.*, *89*, 1147–1163.

Parrish, R. R., and K. V. Hodges (1996), Isotopic constraints on the age and provenance of the Lesser and Greater Himalayan sequences, Nepalese Himalaya, *Geol. Soc. Am. Bull.*, *108*, 904–911.

Patel, R. C., S. Singh, A. Asokan, R. M. Manickavasagam, and A. K. Jain (1993), Extensional tectonics in the Himalayan orogen, Zanskar, NW India, in *Himalayan Tectonics*, edited by P. J. Treloar and M. P. Searle, *Geol. Soc. Spec. Publ.*, *74*, 445–459.

Powers, P. M., R. J. Lillie, and R. S. Yeats (1998), Structure and shortening of the Kangra and Dehra Dun reentrants, Sub-Himalaya, India, *Geol. Soc. Am. Bull.*, *110*, 1010–1027.

Prell, W. L., D. W. Murray, and S. C. Clemens (1992), Evolution and variability of the Indian Ocean summer monsoon: Evidence from the western Arabian sea drilling program, in *Synthesis of Results From Scientific Drilling in the Indian Ocean*, *Geophys. Monogr. Ser.*, vol. 70, edited by R. A. Duncan et al., pp. 447–469, AGU, Washington, D. C.

Rahn, M. K., and B. Grasemann (1999), Fission track and numerical thermal modeling of differential exhumation of the Glarus thrust plane (Switzerland), *Earth Planet. Sci. Lett.*, *169*, 245–259.

Rea, D. K. (1992), Delivery of Himalayan sediment to the northern Indian Ocean and its relation to global climate, sea level, uplift, and sea water strontium, in *Synthesis of Results From Scientific Drilling in the Indian Ocean*, *Geophys. Monogr. Ser.*, vol. 70, edited by R. A. Duncan et al., pp. 387–402, AGU, Washington, D. C.

Renne, P. R., A. L. Deino, R. C. Walter, B. D. Turrin, C. C. Swisher, T. A. Becker, G. H. Curtis, W. D. Sharp, and A. R. Jaouni (1994), Intercalibration of astronomical and radioisotopic time, *Geology*, *22*, 783 – 786.

Robinson, D. M., P. G. De Celles, P. J. Patchett, and C. N. Garzione (2001), The kinematic evolution of the Nepalese Himalaya interpreted from Nd isotopes, *Earth Planet. Sci. Lett.*, *192*, 507 – 521.

Ruddiman, W. F., M. E. Raymo, W. Prell, and J. E. Kutzbach (1997), The uplift-climate connection: A synthesis, in *Global Tectonics and Climate Change*, edited by W. Ruddiman and W. F. Prell, pp. 471 – 515, Plenum, New York.

Ruppel, C., and K. V. Hodges (1994), Pressure-temperature-time paths from two-dimensional thermal models: Prograde, retrograde, and inverted metamorphism, *Tectonics*, *13*, 17 – 44.

Searle, M. P., S. R. Noble, A. J. Hurford, and D. C. Rex (1999), Age of crustal melting, emplacement and exhumation history of the Shivling leucogranite, Garhwal Himalaya, *Geol. Mag.*, *136*, 513 – 525.

Seeber, L., and V. Gornitz (1983), River profiles along the Himalayan arc as indicators of active tectonics, *Tectonophysics*, *92*, 335 – 367.

Sharma, D., A. K. Goel, and R. S. Minhas (1991), Water and sediment yields into the Sutlej River from the High Himalaya, *Mt. Res. Dev.*, *11*(2), 87 – 100.

Shroder, J. F., and M. P. Bishop (2000), Unroofing the Nanga Parbat, in *Tectonics of the Nanga Parbat Syntaxis and the Western Himalaya*, edited by M. A. Khan et al., *Geol. Soc. Spec. Publ.*, *170*, 163 – 179.

Sorkhabi, R. B., E. Stump, K. A. Foland, and A. K. Jain (1996), Fission-track and $^{40}Ar/^{39}Ar$ evidence for episodic denudation of the Gangotri granites in the Garhwal Higher Himalaya, India, *Tectonophysics*, *260*, 187 – 199.

Srikantia, S. V., and O. N. Bhargava (1998), *Geology of Himachal Pradesh*, 406 pp., Geol. Soc. of India, Bangalore.

Srivastava, P., and G. Mitra (1994), Thrust geometries and deep structure of the outer and lesser Himalaya, Kumaon and Garhwal (India): Implications for evolution of the Himalayan fold-and-thrust belt, *Tectonics*, *13*, 89 – 109.

Tagami, T., R. F. Galbraith, R. Yamada, and G. M. Laslett (1998), Revised annealing kinematics of fission tracks in zircon and geological implications, in *Advances in Fission Track Geochronology*, edited by F. De Corte and P. Van den Haute, pp. 99 – 112, Kluwer Acad., Norwell, Mass.

Upreti, B. N., and P. Le Fort (1999), Lesser Himalayan crystalline nappes of Nepal: Problems of their origin, in *Himalaya and Tibet*: *Mountain Roots to Mountain Tops*, edited by A. Macfarlane, R. B. Sorkhabi, and J. Quade, *Spec. Pap. Geol. Soc. Am.*, *328*, 225 – 238.

Valdiya, K. S. (1980), The two intracrustal boundary thrusts of the Himalaya, *Tectonophysics*, *66*, 323 – 348.

Vance, D., and N. Harris (1999), Timing of prograde metamorphism in the Zanskar Himalaya, *Geology*, *27*, 395 – 398.

Vance, D., M. Bickle, S. Ivy-Ochs, and P. W. Kubick (2003), Erosion and exhumation in the Himalaya from cosmogenic isotope inventories of river sediments, *Earth Planet. Sci. Lett.*, *206*, 273 – 288.

Vannay, J.-C., and B. Grasemann (1998), Inverted metamorphism in the High Himalaya of Himachal Pradesh (NW India): Phase equilibria versus thermobarometry, *Schweiz. Mineral. Petrogr. Mitt.*, *78*, 107 – 132.

Vannay, J.-C., and B. Grasemann (2001), Himalayan inverted metamorphism and syn-convergence extension as a consequence of a general shear extrusion, *Geol. Mag.*, *138*, 253 – 276.

Vannay, J.-C., and K. V. Hodges (1996), Tectonometamorphic evolution of the Himalayan metamorphic core between the Annapurna and Dhaulagiri, central Nepal, *J. Metamorph. Geol.*, *14*, 635 – 656.

Vannay, J.-C., and A. Steck (1995), Tectonic evolution of the High Himalaya in Upper Lahul (NW Himalaya India), *Tectonics*, *14*, 253 – 263.

Vannay, J.-C., Z. D. Sharp, and B. Grasemann (1999), Himalayan inverted metamorphism constrained by oxygen isotope thermometry, *Contrib. Mineral. Petrol.*, *137*, 90 – 101.

White, N. M., M. Pringle, E. Garzanti, M. Bickle, Y. Najman, H. Chapman, and P. Friend (2002), Constraints on the exhumation and erosion of the High Himalayan Slab, NW India, from foreland basin deposits, *Earth Planet. Sci. Lett.*, *195*, 29 – 44.

Whittington, A., N. B. W. Harris, M. W. Ayres, and G. Foster (2000), Tracing the origin of the western Himalaya: An isotopic comparison of the Nanga Parbat massif and Zanskar Himalaya, in *Tectonics of the Nanga Parbat Syntaxis and the Western Himalaya*, edited by M. A. Khan et al., *Geol. Soc. Spec. Publ.*, *170*, 201 – 218.

Wiesmayr, G., and B. Grasemann (2002), Eohimalayan fold and thrust belt: Implications for the geo dynamic evolution of the NW-Himalaya (India), *Tectonics*, *21*(6), 1058, doi:10.1029/2002TC001363.

Zeitler, P. K., et al. (2001), Crustal reworking at Nanga Parbat, Pakistan: Metamorphic consequence of thermal-mechanical coupling facilitated by erosion, *Tectonics*, *20*, 712 – 728.

V. Baudraz, M. Cosca, and J.-C. Vannay, Institut de Minéralogie et Géochimie, Université de Lausanne, CH-1015 Lausanne, Switzerland. (jean-claude.vannay@img.unil.ch)

A. Carter, Research School of Geological and Geophysical Sciences, Birkbeck and University Colleges London, Gower Street, London WC1E 6BT, UK.

B. Grasemann and W. Frank, Institut für Geologie, Universität Wien, Althanstrasse 14, A-1090 Vienna, Austria.

M. Rahn, Swiss Federal Nuclear Safety Inspectorate (HSK), CH-5232 Villigen-HSK, Switzerland.